



BREAKTHROUGH REPORT

Cellular Ca²⁺ Signals Generate Defined pH Signatures in Plants^[OPEN]

Smrutisanjita Behera,^{a,b,1} Zhaolong Xu,^{a,c,1} Laura Luoni,^{a,1} Maria Cristina Bonza,^{a,1} Fabrizio Gandolfo Doccia,^a Maria Ida De Michelis,^a Richard J. Morris,^{d,1} Markus Schwarzländer,^{e,1} and Alex Costa^{a,f,2}^a Department of Biosciences, University of Milan, 20133 Milan, Italy^b Indian Institute of Chemical Biology, Council of Scientific and Industrial Research, 700 032 West Bengal, India^c Salt-Soil Agricultural Center, Institute of Agricultural Resources and Environment, Jiangsu Academy of Agricultural Sciences, Nanjing 210014, China^d Computational and Systems Biology, John Innes Centre, Norwich Research Park, Norwich NR4 7UH, UK^e Institute for Biology and Biotechnology of Plants, University of Münster, 48143 Münster, Germany^f Institute of Biophysics, Consiglio Nazionale delle Ricerche, 20133 Milan, Italy

ORCID IDs: 0000-0001-8749-6130 (S.B.); 0000-0002-7374-7303 (Z.X.); 0000-0002-6485-5417 (L.L.); 0000-0001-7096-2967 (M.C.B.); 0000-0002-4499-2297 (F.G.D.); 000-0001-7684-9252 (M.I.D.M.); 0000-0003-3080-2613 (R.J.M.); 0000-0003-0796-8308 (M.S.); 0000-0002-2628-1176 (A.C.)

Ca²⁺ play a key role in cell signaling across organisms. The question of how a simple ion can mediate specific outcomes has spurred research into the role of Ca²⁺ signatures and their encoding and decoding machinery. Such studies have frequently focused on Ca²⁺ alone and our understanding of how Ca²⁺ signaling is integrated with other responses is poor. Using in vivo imaging with different genetically encoded fluorescent sensors in *Arabidopsis thaliana* cells, we show that Ca²⁺ transients do not occur in isolation but are accompanied by pH changes in the cytosol. We estimate the degree of cytosolic acidification at up to 0.25 pH units in response to external ATP in seedling root tips. We validated this pH-Ca²⁺ link for distinct stimuli. Our data suggest that the association with pH may be a general feature of Ca²⁺ transients that depends on the transient characteristics and the intracellular compartment. These findings suggest a fundamental link between Ca²⁺ and pH dynamics in plant cells, generalizing previous observations of their association in growing pollen tubes and root hairs. Ca²⁺ signatures act in concert with pH signatures, possibly providing an additional layer of cellular signal transduction to tailor signal specificity.

INTRODUCTION

Ca²⁺ are used in signaling by both prokaryotes and eukaryotes (Clapham, 2007). The origin of the signaling functions of Ca²⁺ likely results from its chemical ability to bind and precipitate phosphates, including ATP, a condition that cells must avoid to survive (Sze et al., 2000). As the Ca²⁺ concentration of water is in the millimolar range, which is above the equilibrium dissociation constant of various forms of ATP to Ca²⁺ and would therefore be toxic to the cell, cells have evolved ways to decrease the Ca²⁺ concentration using pumps, transporters, and buffers. Cells typically maintain cytosolic free Ca²⁺ concentrations at resting levels of ~50–200 nM, resulting in a substantial chemical Ca²⁺ gradient among the cytosol, the extracellular space, and intracellular compartments (e.g., vacuole and endoplasmic reticulum) (Stael et al., 2012; Costa et al., 2018). Besides, the net

electrical potentials existing across the plasma membrane (PM) and tonoplast contribute to building up large electrochemical gradients to drive for Ca²⁺ transport. Cells exploit these gradients and the associated machinery to generate rapid intracellular concentration changes, which provide the basis for Ca²⁺ signaling (Sze et al., 2000; Clapham, 2007; Dodd et al., 2010).

The energy required to maintain such a large electrochemical Ca²⁺ gradient is provided by ATP, which is used directly by Ca²⁺-ATPases and indirectly by Ca²⁺ antiporters, such as Ca²⁺/H⁺ exchangers (e.g., CAX proteins), to extrude Ca²⁺ out of the cytosol driven by the proton motive force (Bonza and De Michelis, 2011; Emery et al., 2012; Martins et al., 2013). Using H⁺ gradients generated by P-type and V-type ATPases at both the PM and tonoplast (Serrano, 1989; Gaxiola et al., 2007; Duby and Boutry, 2009), Ca²⁺/H⁺ transporters link the transport of Ca²⁺ with the transport of H⁺. Moreover, Ca²⁺ export via Ca²⁺-ATPases (localized at the PM, tonoplast, endoplasmic reticulum, and Golgi) acts by a net Ca²⁺/H⁺ exchange lowering the energetic requirement for the export (Rasi-Caldogno et al., 1987; Beggagna et al., 2000; Luoni et al., 2000; Brini and Carafoli, 2009; Bonza and De Michelis, 2011).

Other ions move across the membranes. In addition to the CAXs, plants have a large set of predicted cation/H⁺ exchangers localized in the different membranes that may contribute to pH

¹ These authors contributed equally to this work.² Address correspondence to alex.costa@unimi.it.

The author responsible for distribution of materials integral to the findings presented in this article in accordance with the policy described in the Instructions for Authors (www.plantcell.org) is: Alex Costa (alex.costa@unimi.it).

^[OPEN]Articles can be viewed without a subscription.

www.plantcell.org/cgi/doi/10.1105/tpc.18.00655

IN A NUTSHELL

Background: Plants survive by adapting their development and physiology to external changes. Information within cells is commonly encoded in Ca²⁺ signals; different external stimuli are translated into changes in the cytosolic Ca²⁺ concentration. Such Ca²⁺ signals are decoded by a range of Ca²⁺ sensors. An unresolved problem in Ca²⁺ signaling is how a simple ion encodes complex information with high specificity. Ca²⁺ signals may operate in concert with other second messengers, and protons have been suggested as candidates. Several proteins that transport Ca²⁺ across plant membranes also transport protons, and there is evidence from other systems, such as growing pollen tubes, that supports a connection between cytosolic Ca²⁺ and pH dynamics.

Question: Building on a body of previous work, we considered protons as a potential signal and investigated the link with Ca²⁺. We tested the generality of this coupling signaling by monitoring changes in both Ca²⁺ and pH for a variety of external stimuli.

Findings: Using modern imaging microscopy technologies and genetically encoded fluorescent biosensors, we monitored Ca²⁺ and protons at high resolution within living cells and demonstrated that cytosolic Ca²⁺ and pH dynamics are linked in both leaf and root cells of *Arabidopsis* (*Arabidopsis thaliana*) subjected to external stimuli. Specifically, when a cytosolic Ca²⁺ increase occurs, cytosolic pH decreases. In membrane transport mutants and in response to chemical treatments that perturb Ca²⁺ and proton homeostasis, the link was maintained, indicating its robustness. However, the link was modified in cell organelles. Although their internal pH was dominated by the cytosol, Ca²⁺ dynamics differed, pointing to modulation at the subcellular level, which could provide a basis for encoding intracellular signals.

Next steps: We have demonstrated that pH and Ca²⁺ are linked, but the underlying mechanism is unknown. The finding that the responses are similar, but not strictly correlated, and in some cases delayed, points to something more complex than would be expected from a simple transporter model or joint buffers. Using multiparametric imaging across a range of stimuli with further chemical and genetic perturbations coupled with the development of mechanistic models will help unravel these fascinating observations.

changes in response to a change of membrane potential (Sze and Chanroj, 2018). Generally, the membrane potential provides an integrative link between all ions moving across a membrane as described by the Goldman-Hodgkin-Katz equation (Hille, 1992). As such, cytosolic Ca²⁺ increase through influx across a membrane is likely to be associated with a membrane potential change, which will in turn influence H⁺ transport. It can therefore be hypothesized that changes of cytosolic free Ca²⁺ concentration ([Ca²⁺]_{cyt}), because of its influx through channels (Swarbreck et al., 2013), are accompanied by changes in cytosolic pH (pH_{cyt}) possibly linked to its efflux (Bonza and De Michelis, 2011). Indeed, evidence of a link between [Ca²⁺]_{cyt} and pH_{cyt} has been observed in the tip of growing pollen tubes and root hairs (Herrmann and Felle, 1995; Monshausen et al., 2008; Michard et al., 2011, 2017), guard cells in response to ABA (reviewed in Blatt and Grabov, 1997) as well as in seedlings subjected to cold stress (Gao et al., 2004), exogenous auxin (indole-3-acetic acid, IAA) treatment (Dindas et al., 2018) or mechanical stimulation (Monshausen et al., 2009).

To better understand the interaction between cytosolic Ca²⁺ transients and H⁺ homeostasis, we carefully applied the use of fluorescent biosensors to analyze pH and Ca²⁺ dynamics in living plant cells. Using well-defined external stimuli, our results demonstrate that transients in Ca²⁺ are linked with transients in pH in the cytosol. The link was observed in all cells and tissues investigated and it was maintained in mutants of selected candidate mechanisms. The pH transients were remarkably similar in the cytosol, mitochondria, and plastids, despite distinct Ca²⁺ responses. Our data show that Ca²⁺ and pH are linked but not strictly coupled, thus raising the possibility that the pH transient may encode additional information to the Ca²⁺ transient. Our

observations extend the concept of Ca²⁺ signatures to pH, providing insights into their joint response while raising new questions about the mechanistic nature of the coupling and how specificity may be achieved in Ca²⁺ signaling.

RESULTS

To investigate whether the dynamics in [Ca²⁺]_{cyt} are accompanied by pH changes, we monitored pH_{cyt} in *Arabidopsis* (*Arabidopsis thaliana*) leaves subjected to wounding. An early event occurring after wounding of leaf tissue is a fast [Ca²⁺]_{cyt} increase, occurring primarily in the cells that surround the wounded site and then spreading across the leaf as a “Ca²⁺ wave” (Beneloujaephajri et al., 2013). Although it is hard to differentiate between a passive injury response and active Ca²⁺ signaling close to the injury site, the propagated Ca²⁺ wave is clearly a result of activated cytosolic Ca²⁺ transients. To capture the dynamics of the wounding response, we used two separate *Arabidopsis* plant lines expressing the NES-YC3.6 (Nagai et al., 2004; Krebs et al., 2012) and the pH-green fluorescent protein (GFP) (Moseyko and Feldman, 2001; Fendrych et al., 2014) sensors for [Ca²⁺]_{cyt} and pH_{cyt}, respectively (Supplemental Movies 1 and 2). For both Ca²⁺ and pH, we observed reproducible in vivo responses. Increases in [Ca²⁺]_{cyt} were accompanied by cytosolic acidification as illustrated by the superimposed averaged traces from independent experiments normalized to the pre-stimulus level (*R*₀) (Figure 1). Leaf wounding generated the characteristic Ca²⁺ signature featuring two maxima as observed previously (Beneloujaephajri et al., 2013; Costa et al., 2017) (Figure 1A, Supplemental Movie 1). The first maximum showed a sharp onset and decline with a high amplitude and

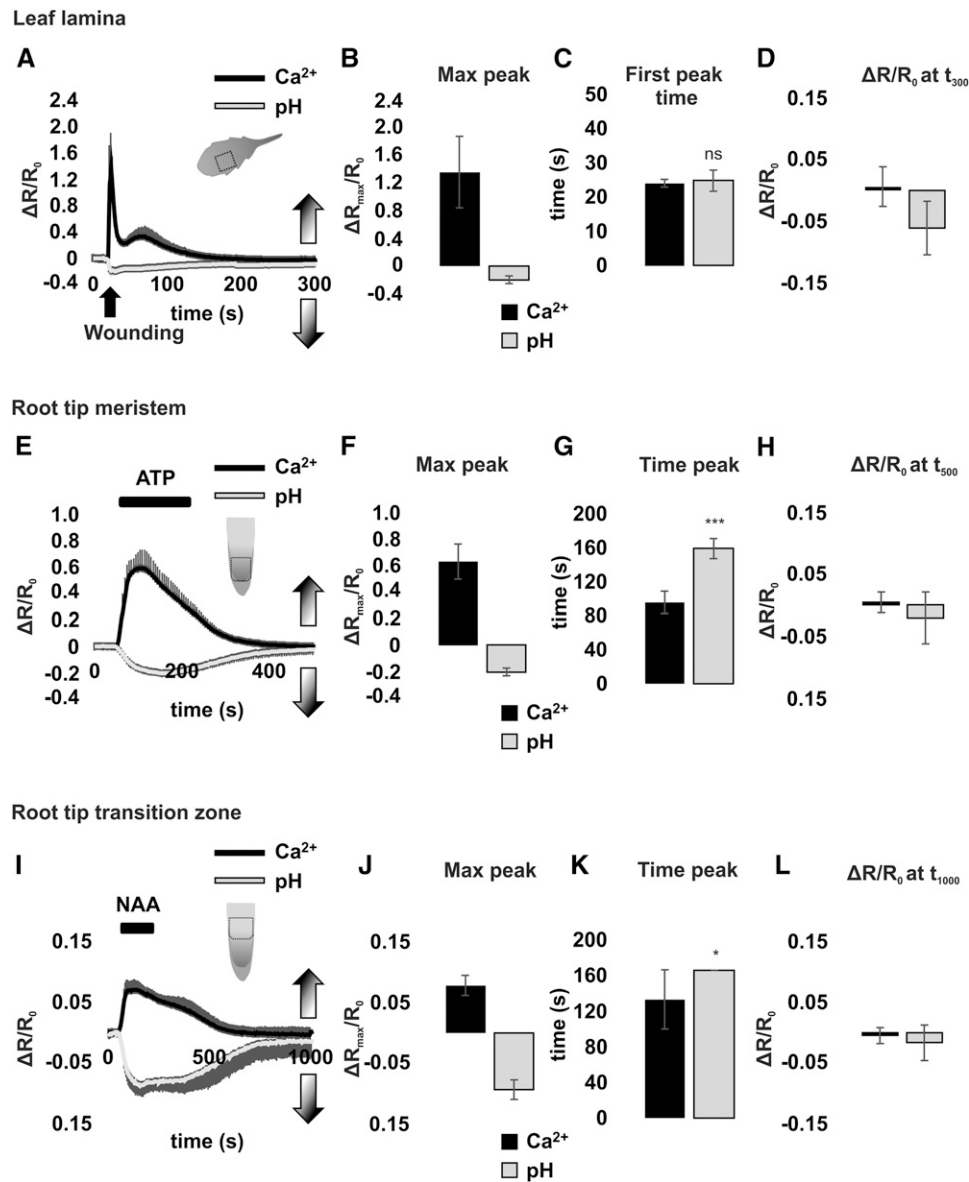


Figure 1. Cytosolic Ca²⁺ Transients in Response to Wounding, External ATP, and NAA Are Accompanied by Changes to Cytosolic pH.

(A) Averaged cpVenus/CFP (Ca²⁺, black) and 405_{ex}/488_{ex} (pH, gray) ratios of the ROI (schematic drawing), corresponding to the cells surrounding the wounded leaf area, are plotted over time and reported as $\Delta R/R_0$.

(B) First peak cpVenus/CFP and 405_{ex}/488_{ex} ratios as $\Delta R/R_0$ maximum increase or decrease after wounding.

(C) Time when $\Delta R_{max}/R_0$ increase after wounding is reached.

(D) Amplitudes of cpVenus/CFP and 405_{ex}/488_{ex} ratios reported as $\Delta R/R_0$ of cells close to the wounding region at 300 s.

(E) Averaged cpVenus/CFP (Ca²⁺, black) and 405_{ex}/488_{ex} (pH, gray) ratios of the ROI (schematic drawing), corresponding to the root tip meristem treated with 0.1 mM ATP, are plotted over time and reported as $\Delta R/R_0$.

(F) Peak cpVenus/CFP and 405_{ex}/488_{ex} ratios as $\Delta R/R_0$ maximum increase or decrease after ATP treatment.

(G) Time when $\Delta R_{max}/R_0$ increase after ATP treatment is reached.

(H) Amplitudes of cpVenus/CFP and 405_{ex}/488_{ex} ratios reported as $\Delta R/R_0$ at 500 s.

(I) Averaged cpVenus/CFP (Ca²⁺, black) and 405_{ex}/488_{ex} (pH, gray) ratios of the ROI (schematic drawing), corresponding to the root tip transition zone treated with 0.01 mM NAA, are plotted over time and reported as $\Delta R/R_0$.

(J) Peak cpVenus/CFP and 405_{ex}/488_{ex} ratios as $\Delta R/R_0$ maximum increase or decrease after NAA treatment.

(K) Time when $\Delta R_{max}/R_0$ increase after NAA treatment is reached.

(L) Amplitudes of cpVenus/CFP and 405_{ex}/488_{ex} ratios reported as $\Delta R/R_0$ at 1000 s.

Shaded arrows up represent Ca²⁺ increase; shaded arrows down represent pH decrease. $n \geq 5$; * $P \leq 0.05$, ** $P \leq 0.01$, *** $P \leq 0.001$ (t test); error bars = sd.

peaked at 24 ± 1 s after the stimulus, whereas the second showed slower kinetics, a lower amplitude, and peaked at 66 ± 11 s (Figures 1A to 1C). $[Ca^{2+}]_{\text{cyt}}$ levels recovered to the resting values at ~ 250 s after the stimulus (Figure 1D). The same experiment was performed with plants expressing the pH sensor (Figure 1A, Supplemental Figures 1A to 1D, Supplemental Movies 2 and 3). Leaf wounding induced cytosolic acidification (Figures 1A to 1D and Supplemental Movie 2) with a pH minimum (Figures 1A and 1B) that occurred at a time not significantly different from the first Ca²⁺ peak (25 ± 3 s, Figure 1C). For the second Ca²⁺ peak, however, no distinct pH response could be resolved. Despite differences in shape, the pH_{cyt} recovered to resting values at ~ 250 s after the stimulus, coincidentally with the recovery of the resting $[Ca^{2+}]_{\text{cyt}}$. These observations demonstrate that leaf wounding induces a Ca²⁺ transient in the cells surrounding the damaged site that shares several features with a pH transient, but that pH_{cyt} changes do not strictly mirror $[Ca^{2+}]_{\text{cyt}}$ dynamics.

To investigate whether our observations are specific to wounding or of more general relevance, we repeated the experiment using extracellular ATP. ATP is released from mechanically damaged cells during wounding, acting as a damage-associated molecular pattern (Cao et al., 2014; Choi et al., 2014; Tanaka et al., 2014). Extracellular ATP can be sensed, for instance, by root tip cells, where it triggers a fast and sustained $[Ca^{2+}]_{\text{cyt}}$ increase (Tanaka et al., 2010; Loro et al., 2012; Waadt et al., 2017). For the following experiments, we made use of a custom perfusion setup for fluorescence in vivo microscopy imaging in Arabidopsis seedling roots (Behera and Kudla, 2013; Bonza et al., 2013; Wagner et al., 2015a) (Figures 1E to 1L). ATP administration at 0.1 mM to the seedlings expressing NES-YC3.6 triggered a steep rise in $[Ca^{2+}]_{\text{cyt}}$. Transient cytosolic acidification was observed in seedlings expressing pH-GFP, similarly to the acidification in response to the wounding stimulus (Figures 1E and 1F, Supplemental Movies 4 and 5). However, the maximal responses of the two transients did not coincide; $[Ca^{2+}]_{\text{cyt}}$ peaked at 95 ± 13 s after ATP application whereas the maximal acidification occurred later, at 159 ± 12 s (Figure 1G). At recovery, the pre-stimulus Ca²⁺ and pH levels were both reached after approximately 450 s (Figure 1H). This experiment confirms an association between $[Ca^{2+}]_{\text{cyt}}$ and pH_{cyt} dynamics, whereas the temporal difference in reaching the maxima highlights that a direct mechanistic coupling is unlikely but is instead mediated by interacting physiological activities (Felle, 2001). In a simplistic view, the delay of the minimum pH might be explained by its main association with the Ca²⁺ efflux phase (mediated by cation/H⁺ exchangers, CAXs and Ca²⁺-ATPases) and not with the influx phase (mediate by Ca²⁺-permeable channels).

As a third assessment of the interplay between $[Ca^{2+}]_{\text{cyt}}$ and pH, we monitored their dynamics in root cells of the transition zone in response to administration of the synthetic auxin 1-naphthaleneacetic acid (NAA) (0.01 mM) (Figures 1I to 1L, Supplemental Movies 6 and 7). The natural auxin IAA has been previously shown to induce a $[Ca^{2+}]_{\text{cyt}}$ transient (Monshausen et al., 2011; Shih et al., 2014, 2015; Waadt et al., 2017) and simultaneous apoplastic alkalization in root cells (Monshausen et al., 2011; Gjetting et al., 2012; Shih et al., 2014, 2015). Recently, Dindas et al. (2018) reported a cytosolic H⁺ influx in

IAA-treated root cells. Our data show that NAA treatment of seedling roots results in both a $[Ca^{2+}]_{\text{cyt}}$ increase and a pH_{cyt} decrease (Figure 1I), albeit with different signatures from those recorded after ATP administration (Figure 1E). The averaged traces from the Ca²⁺ and the pH sensor almost mirror each other, but with a delayed pH_{cyt} minimum as compared with the $[Ca^{2+}]_{\text{cyt}}$ maximum (133 ± 33 s for Ca²⁺ versus 166 ± 26 s for pH, $P < 0.05$; Figure 1K). At recovery, the pre-stimulus levels of both parameters were regained almost simultaneously (after ~ 950 s), consistent with the other two stimuli (Figure 1L). The inverse pH changes on both sides of the PM may conceivably be part of the same process via transport of H⁺ across the PM. Thus, the NAA-induced cytosolic acidification may contribute to the previous observation of apoplastic alkalization dependent on a $[Ca^{2+}]_{\text{cyt}}$ increase (Monshausen et al., 2011; Gjetting et al., 2012; Shih et al., 2014, 2015). Although our observations point to a general link between $[Ca^{2+}]_{\text{cyt}}$ and pH_{cyt}, we cannot rule out that NAA may also directly affect the activity of the H⁺ pumping ATPase, to influence both cytosolic and apoplastic pH (Barbez et al., 2017). A role of AUX1-mediated IAA transport ($2H^+/IAA^-$) in cytosolic acidification has been recently postulated, suggesting that at least in part the observed acidification is because of the IAA transport itself (Dindas et al., 2018). However, NAA is not a substrate of AUX1 (Yang et al., 2006); thus, further work is needed to disentangle the causality of the events among NAA, Ca²⁺, and pH dynamics.

The responses of different plant cell types to different stimuli show the common feature that the induced $[Ca^{2+}]_{\text{cyt}}$ increase is accompanied by an increase in the cytosolic proton concentration $[H^+]_{\text{cyt}}$ and that the recovery to the pre-stimulus conditions is temporally synchronized, supporting the idea that both parameters are also linked mechanistically. The different responses of $[Ca^{2+}]_{\text{cyt}}$ and pH_{cyt} to different stimuli, the absence of a second pH peak upon wounding, and the shift in the maximal responses between $[Ca^{2+}]_{\text{cyt}}$ and pH_{cyt} for ATP and NAA suggest that the link is not direct, as would, for instance, be expected for a buffer exchange mechanism (Plieth et al., 1997) or for a Ca²⁺/H⁺ exchange across the PM or another membrane. Moreover, it can also be taken into consideration that Ca²⁺/H⁺ exchange systems should contribute only to the $[Ca^{2+}]_{\text{cyt}}$ recovery phase and not to Ca²⁺ influx, which is putatively mediated by channels.

To further test the hypothesis that the cytosolic pH changes are linked to cytosolic Ca²⁺ changes, we aimed at modifying the dynamic/magnitude of the ATP-induced $[Ca^{2+}]_{\text{cyt}}$ increase in root tip cells. It has been reported that this ATP-induced Ca²⁺ transient has a primary component because of the influx of Ca²⁺ from the apoplast together with a secondary release of Ca²⁺ from interior stores (Tanaka et al., 2010). Thus, we transiently supplemented the imaging solution with 1 mM of EGTA to chelate and thus reduce the free Ca²⁺ availability in the extracellular space (Figure 2A). In this condition, ATP administration still triggered an increase in $[Ca^{2+}]_{\text{cyt}}$, but its amplitude was strongly reduced as compared with the non-chelator control (Figure 1E). The ATP-induced pH_{cyt} decrease showed an analogous reduction in amplitude (Figures 2A and 2B). Subsequent EGTA washout re-established the typical $[Ca^{2+}]_{\text{cyt}}$ and pH_{cyt} changes of the control (Figures 2A and 2B), providing evidence for causal linkage in which the amplitude of the change in $[Ca^{2+}]_{\text{cyt}}$ determines the amplitude of the pH change.

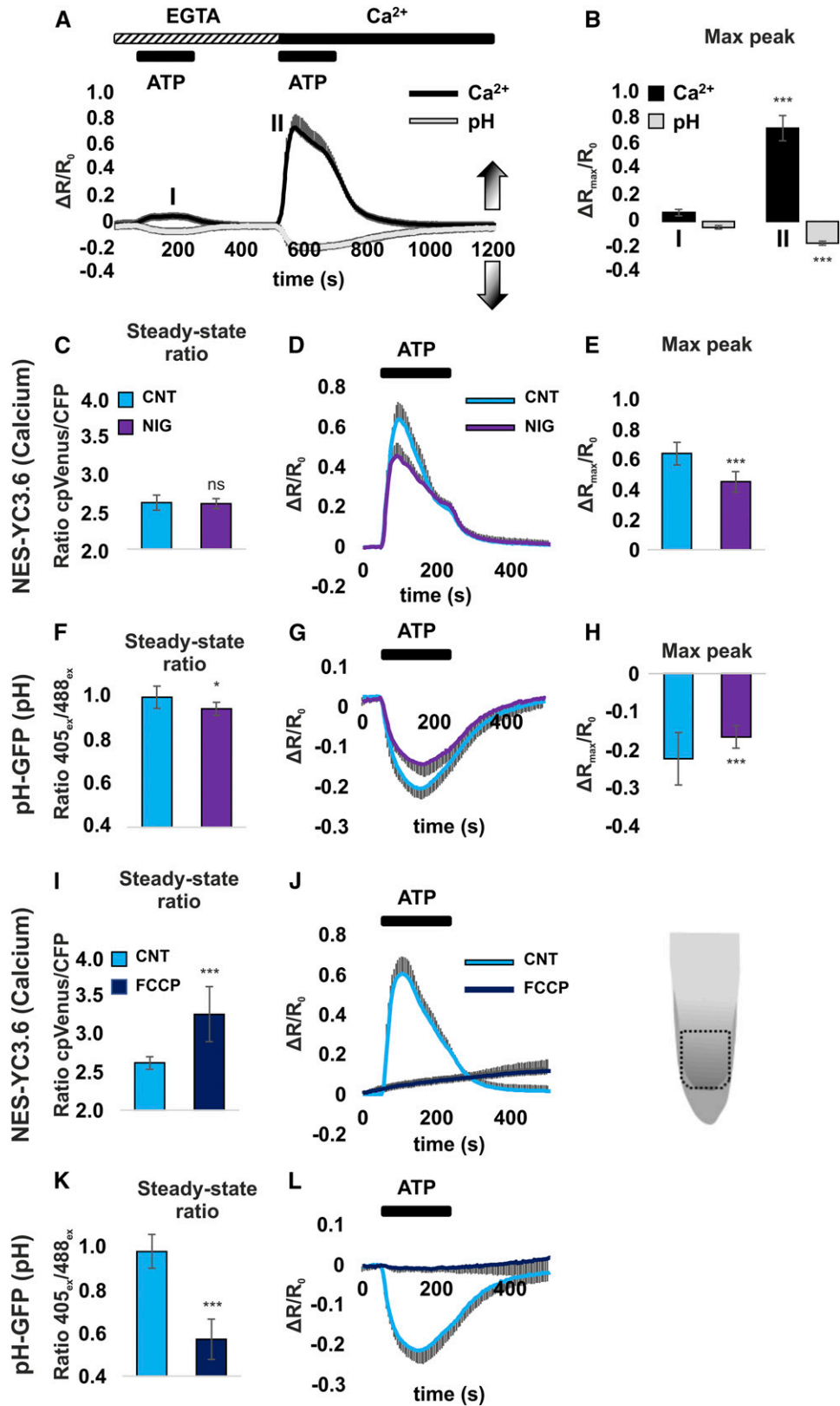


Figure 2. Extracellular Ca²⁺ Chelation with EGTA Affects Both Ca²⁺ and pH Cytosolic Transients Induced by External ATP.

To shed light on the nature of the link between [Ca²⁺]_{cyt} and pH_{cyt}, we adopted a pharmacological and a genetic approach. First, we aimed to manipulate pH_{cyt} as a primary modification to assess whether it affects [Ca²⁺]_{cyt}. We clamped cytosolic pH or dissipated H⁺ gradients across cellular membranes by pre-treating the Arabidopsis seedlings (expressing NES-YC3.6 and pH-GFP) with 5 μM of the ionophore nigericin (acting mainly as a H⁺/K⁺ exchanger) (Figures 2C to 2H) or 5 μM of the protonophore Carbonyl cyanide-4-(trifluoromethoxy)phenylhydrazone (FCCP) for 10 min, respectively (Figures 2I to 2L). The treatment with nigericin did not affect the resting [Ca²⁺]_{cyt} (Figure 2C), and only slightly acidified the cytosol (Figure 2F). When nigericin-pre-treated NES-YC3.6 and pH-GFP seedlings were exposed to external ATP, a reduced magnitude of both Ca²⁺ maximum (Figures 2D and 2E) and pH minimum transients (Figures 2G and 2H) was observed. In both cases, the time of the peaks was not affected (95 ± 6 control (CNT) versus 95 ± 10 NIG for Ca²⁺ and 155 ± 13 CNT versus 162 ± 11 NIG for pH). Thus, nigericin did not break the [Ca²⁺]_{cyt} and pH_{cyt} link, only affecting the magnitude of the maximum and minimum of the transients. FCCP treatment induced cytosolic acidification (estimated as ~0.2 pH units, Supplemental Figure 1) but also an increase of the [Ca²⁺]_{cyt} compared with the control conditions (Figures 2I and 2K). In the presence of FCCP, the seedlings failed to show any [Ca²⁺]_{cyt} increase and acidification at ATP exposure (Figures 2J and 2L). FCCP pre-treatment severely compromises membrane energetics, which is the likely reason for the lack of ATP responses. Nonetheless, the increase in [Ca²⁺]_{cyt} as a consequence of the primary dissipation of the proton gradient (Figures 2I and 2K) confirms a link between the dynamics of the two ions.

We next aimed to manipulate [Ca²⁺]_{cyt} to assess the impact on pH_{cyt}. Although the Ca²⁺-ATPase inhibitor EosY provides a straightforward pharmacological means of in vivo interference with cytosolic Ca²⁺ homeostasis (Bonza et al., 2013), the fluorescence of EosY cannot be easily separated from that of the

pH-GFP sensor, compromising quantitative measurements (De Vriese et al., 2018). We therefore decided to follow a genetic approach by selecting two different Arabidopsis Ca²⁺-ATPase double mutants, *aca8 aca10* (Frei dit Frey et al., 2012) (and *aca4 aca11* (Boursiac et al., 2010). ACA8 and ACA10 are PM-localized IIB Ca²⁺-ATPases and the double *aca8 aca10* mutant has shown different phenotypes related to Ca²⁺ homeostasis, pathogen response, and stomata aperture (Frei dit Frey et al., 2012; Yang et al., 2017; Yu et al., 2018). By contrast, ACA4 and ACA11 are IIB Ca²⁺-ATPases localized at the vacuole membrane and the double mutant shows a high frequency of hypersensitive response-like lesions and altered ion homeostasis (Boursiac et al., 2010). We hypothesized that these mutants might have reduced Ca²⁺ pumping capacity, resulting in a slowed down recovery of the [Ca²⁺]_{cyt} transient and possibly higher basal [Ca²⁺]_{cyt} levels, thus offering a means to genetically perturb the [Ca²⁺]_{cyt} response and to investigate the impact on pH_{cyt}.

We started our analyses with the *aca8 aca10* mutant (expressing the NES-YC3.6 sensor), which was assayed side by side with the Columbia (Col-0) wild-type control for ATP-induced cytosolic Ca²⁺ and pH transients (Figure 3). Resting [Ca²⁺]_{cyt} was not changed in the *aca8 aca10* background, as indicated by similar cpVenus/cyan fluorescent protein (CFP) ratios in the root tip cells of young seedlings (Figure 3A) and suggestive of sufficient backup by other mechanisms for steady-state maintenance in young seedlings. External ATP stimulation of the *aca8 aca10* NES-YC3.6 seedlings led to an altered Ca²⁺ signature as compared with the wild type (Figure 3B); however, with a decreased amplitude (Figure 3C), a lower rate of [Ca²⁺]_{cyt} increase (Figures 3E and 3F) and a delayed recovery to the pre-stimulus level (Figure 3G). Whereas delayed recovery may be intuitively expected in the absence of two important mediators of Ca²⁺ extrusion, a reduced Ca²⁺ amplitude suggests a degree of acclimation in the mutants through modified expression and/or

Figure 2. (continued).

- (A) Averaged cpVenus/CFP (Ca²⁺, black) and 405_{ex}/488_{ex} (pH, gray) ratios of the ROI shown in the right bottom schematic drawing, corresponding to the root tip meristematic cells treated with 0.1 mM ATP, in the presence of 1 mM EGTA or 10 mM CaCl₂, are plotted over time and reported as ΔR/R₀ ± sd variations.
- (B) Peak cpVenus/CFP and 405_{ex}/488_{ex} ratios as ΔR/R₀ maximum increase or decrease after ATP treatment.
- (C) Steady-state cpVenus/CFP ratios preceding ATP administration (averaged over 50-s time window) in CNT (turquoise) and NIG-treated seedlings (purple).
- (D) CNT and NIG-treated root tips of seedlings expressing NES-YC3.6 under continuous perfusion and treated with 0.1 mM ATP for 3 min. Normalized cpVenus/CFP ratios of the ROI shown in the right bottom schematic drawing, are plotted over time.
- (E) Peak cpVenus/CFP ratios as ΔR/R₀ maximum increase after ATP administration.
- (F) Steady-state 405_{ex}/488_{ex} ratios preceding ATP application (averaged over 50-s time window) in CNT (turquoise) and NIG-treated seedlings (purple).
- (G) CNT and NIG-treated root tips of seedlings expressing pH-GFP imaged under continuous perfusion and treated with 0.1 mM ATP for 3 min. Normalized 405_{ex}/488_{ex} ratios of the ROI shown in the right bottom schematic drawing, are plotted over time.
- (H) Peak 405_{ex}/488_{ex} ratios as ΔR/R₀ maximum decrease after ATP administration.
- (I) Steady-state cpVenus/CFP ratios preceding ATP administration (averaged over 50-s time window) in CNT (turquoise) and FCCP-treated seedlings (dark blue).
- (J) CNT and FCCP-treated root tips of seedlings expressing NES-YC3.6 under continuous perfusion and treated with 0.1 mM ATP for 3 min. Normalized cpVenus/CFP ratios of the ROI shown in the right bottom schematic drawing, are plotted over time.
- (K) Steady-state 405_{ex}/488_{ex} ratios preceding ATP application (averaged over 50-s time window) in CNT (turquoise) and FCCP-treated seedlings (dark blue).
- (L) CNT and FCCP-treated root tips of seedlings expressing pH-GFP imaged under continuous perfusion and treated with 0.1 mM ATP for 3 min. Normalized 405_{ex}/488_{ex} ratios of the ROI shown in the inset are plotted over time. CNT = control; NIG = 5 μM nigericin pretreatment; FCCP = 5 μM FCCP pretreatment. *n* ≥ 5; error bars = sd; **P* ≤ 0.05; ****P* ≤ 0.001 (*t* test).

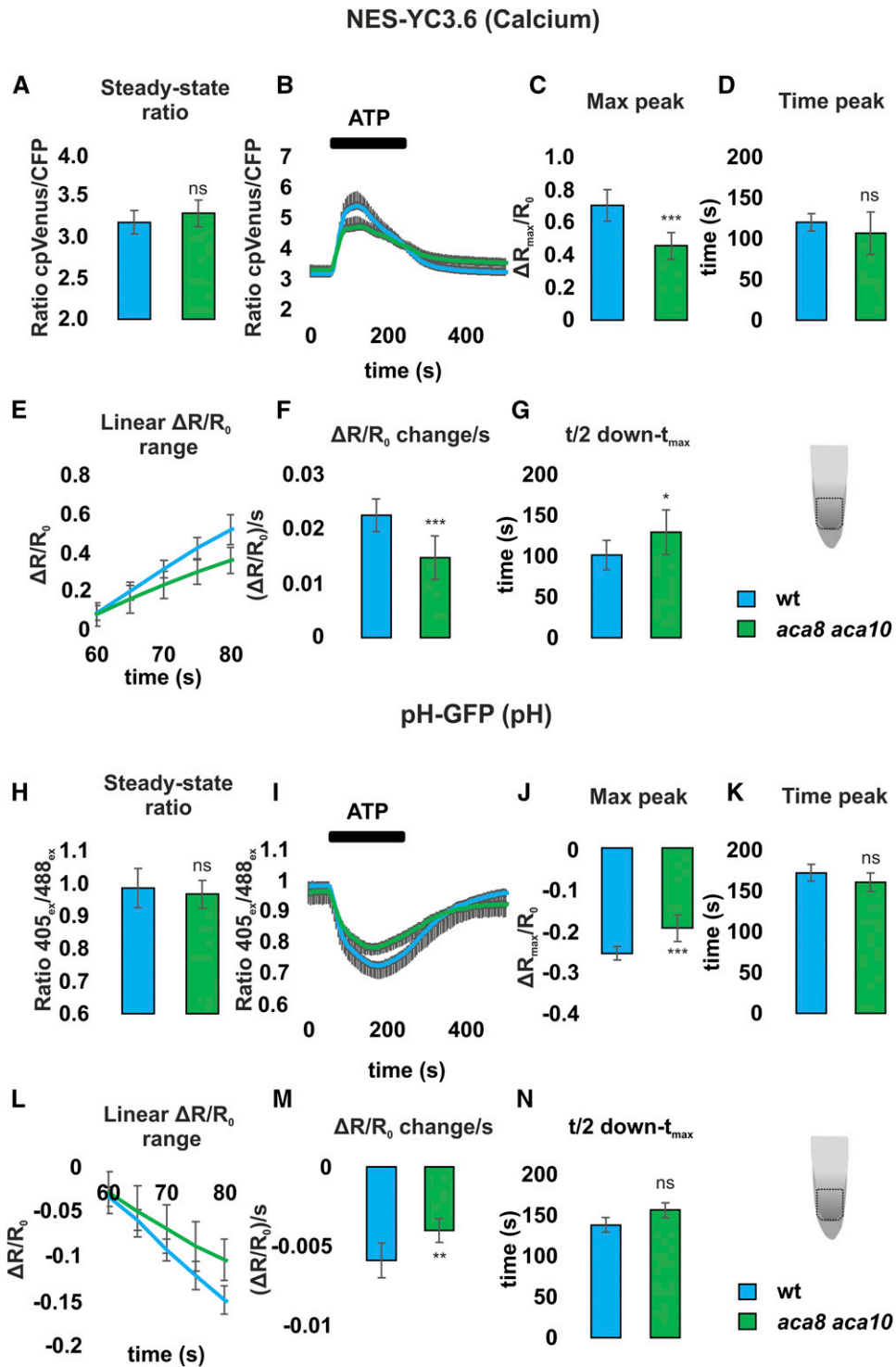


Figure 3. Genetic Ablation of ACA8 and ACA10 Ca²⁺-ATPase Alters Both Ca²⁺ and pH Cytosolic Transients Induced by External ATP.

(A) Steady-state cpVenus/CFP ratios preceding ATP administration (averaged over 50-s time window) of wild type (turquoise) and *aca8 aca10* (green). (B) Root tips of seedlings expressing NES-YC3.6 in wild type and *aca8 aca10* imaged under continuous perfusion and treated with 0.1 mM ATP for 3 min. cpVenus/CFP ratios of the ROI shown in the inset (schematic drawing) are plotted over time. (C) Peak cpVenus/CFP ratios as $\Delta R/R_0$ maximum increase after ATP administration. (D) Time when $\Delta R_{max}/R_0$ increase after ATP administration is reached.

activity of other Ca²⁺ transport mechanisms acting at both the PM and interior membranes. This behavior matches similar observations using aequorin-based Ca²⁺ sensing following flg22 and chitin treatments (Frei dit Frey et al., 2012). When the same experiments were repeated with the pH-GFP sensor lines, we observed analogous differences for the pH transients, with no significant difference in the resting maximum pH_{cyt} as reported by raw 405_{ex}/488_{ex} ratios (Figure 3H), a decreased amplitude of acidification (Figure 3I), and a decreased acidification rate (Figures 3L and 3M), although the pH recovery to pre-stimulus levels was not significantly delayed (Figure 3N). These findings suggest that Ca²⁺ fluxes remain tightly linked to the H⁺ fluxes involved in cytoplasmic acidification. pH recovery appears to depend on the activity of distinct mechanisms, such as activity of the PM and possibly tonoplast H⁺-ATPases. Although the mechanistic impact of the lack of two PM Ca²⁺ pumps is not straightforward to interpret and likely includes pleiotropic components, these results further demonstrate that alteration of the Ca²⁺ dynamic is mirrored by pH change. The similarities between the averaged traces of Ca²⁺ and pH dynamics from the two genetic backgrounds appear particularly evident when superimposed (Supplemental Figure 2).

Side by side analyses of the *aca4 aca11* background with the Col-0 wild-type control for ATP-induced cytosolic Ca²⁺ and pH transients did not reveal any clear difference (Supplemental Figure 3). Lack of the two tonoplast Ca²⁺-ATPases did not alter the resting [Ca²⁺]_{cyt} and pH_{cyt} compared with the wild type (Supplemental Figures 3A and 3H), whereas the maximum peaks of [Ca²⁺]_{cyt} (Supplemental Figure 3C) and the rate of pH_{cyt} decrease (Supplemental Figures 3M and S3N) were slightly altered. Clearly, at least in young seedling root tips, the lack of the two vacuole Ca²⁺-ATPases did not have any major effect on Ca²⁺ and pH dynamics in response to an external ATP stimulus.

Recent work has shown that Ca²⁺ transients in the cytosol trigger Ca²⁺ increases also in intracellular compartments, where the transients display distinct characteristics (Loro et al., 2012, 2016; Wagner et al., 2015a). To assess if the Ca²⁺-pH link that we observed in the cytosol also occurs in other intracellular compartments, we next aimed to assess the interdependency of mitochondrial and plastidic Ca²⁺ and pH in response to the extracellular ATP treatment. Ca²⁺ and pH are thought to be linked by mitochondrial metabolism and energy transformation, which has been studied at depth in mammalian cells (Wagner et al., 2016). In chloroplasts, pronounced changes in pH result from the activity of

the thylakoid electron transport chain, and considerable changes in stromal Ca²⁺ concentration have been observed (Loro et al., 2016). Potential mechanistic links between both are currently under investigation (Carraretto et al., 2016; Armbruster et al., 2017). We compared the responses of three different Arabidopsis sensor lines expressing YC3.6 in the cytosol (NES-YC3.6), mitochondria (4mt-YC3.6), and plastids (2Bam4-YC3.6) after exposing root tips to external ATP (Figures 4A to 4G). Mitochondria showed higher resting cpVenus/CFP ratios than the cytosol, whereas the ratios in the plastid stroma were lower than in the cytosol (Figure 4A). The organelles further showed distinct Ca²⁺ transient kinetics (Figure 4B) as confirmed by different maximum Ca²⁺ peaks (Figure 4D) and different times at which the maximum Ca²⁺ accumulation occurred (Figure 4E). Moreover, the rates of Ca²⁺ accumulation in the mitochondrial matrix and plastid stroma were different from those in the cytosol (Figures 4E and 4F). The recovery times of the cytosol and the plastids were similar, whereas mitochondrial recovery was slower (Figure 4G). As such, the three compartments presented obvious differences in their detectable Ca²⁺ dynamics in response to the same ATP stimulus (Supplemental Figure 4), in agreement with previous findings (Logan and Knight, 2003; Loro et al., 2012, 2016; Wagner et al., 2015a). We then performed analogous experiments for pH, comparing the dynamics in those three compartments (Supplemental Figure 4). We used the MT-cpYFP line in which the high-sensitivity, high-pKa pH sensor cpYFP (circularly permuted yellow fluorescent protein) is targeted to the mitochondrial matrix (Schwarzländer et al., 2011, 2012, 2014). To have comparable results among the different compartments, we then generated Arabidopsis plants expressing the cpYFP localized to the cytosol and the nucleus (C-cpYFP) and to the plastid stroma (as achieved through N-terminal fusion with the tobacco transketolase targeting peptide (TKTP-cpYFP)). Both C-cpYFP and TKTP-cpYFP plants showed appropriate expression of the sensors in root tip cells (Supplemental Figure 5) and the expected subcellular localizations (cytosolic and nuclear in the case of cpYFP and chloroplast in the case of TKTP-cpYFP; Supplemental Figure 6).

To allow for a rigorous analysis, we tested the *in vivo* pH sensitivity of the cpYFP sensor with our experimental setup, by assaying the responses of the seedling root cells expressing the cytosolic cpYFP sensor to different external pH buffer solutions and comparing it with that of pH-GFP (Supplemental Figures 1E to 1H and Supplemental Movie 8; note that for cpYFP a decrease in the 488_{ex}/405_{ex} ratio represents a pH decrease, whereas the

Figure 3. (continued).

(E) cpVenus/CFP ratio expressed as $\Delta R/R_0$ increase following ATP administration; linear region was selected with $R^2 > 0.998$.

(F) Linear rate representing slope of regression of **(E)**.

(G) Time to pass half-maximal ratio during recovery.

(H) Steady-state 405_{ex}/488_{ex} ratios preceding ATP application (averaged over 50-s time window) in wild type (turquoise) and *aca8 aca10* (green).

(I) Root tips of seedlings expressing pH-GFP in wild type and *aca8 aca10* imaged under continuous perfusion and treated with 0.1 mM ATP for 3 min. 405_{ex}/488_{ex} ratios of the ROI shown in the inset (schematic drawing) are plotted over time.

(J) Peak 405_{ex}/488_{ex} ratios as $\Delta R/R_0$ maximum decrease after ATP administration.

(K) Time when as $\Delta R_{\max}/R_0$ decrease after ATP administration is reached.

(L) 405_{ex}/488_{ex} ratio expressed as $\Delta R/R_0$ decrease following ATP administration; linear region was selected with $R^2 > 0.998$.

(M) Linear rate representing slope of regression of **(L)**.

(N) Time to pass half-maximal ratio during recovery. $n \geq 7$; * $P \leq 0.05$, ** $P \leq 0.01$, and *** $P \leq 0.001$ (*t* test); error bars = sd.

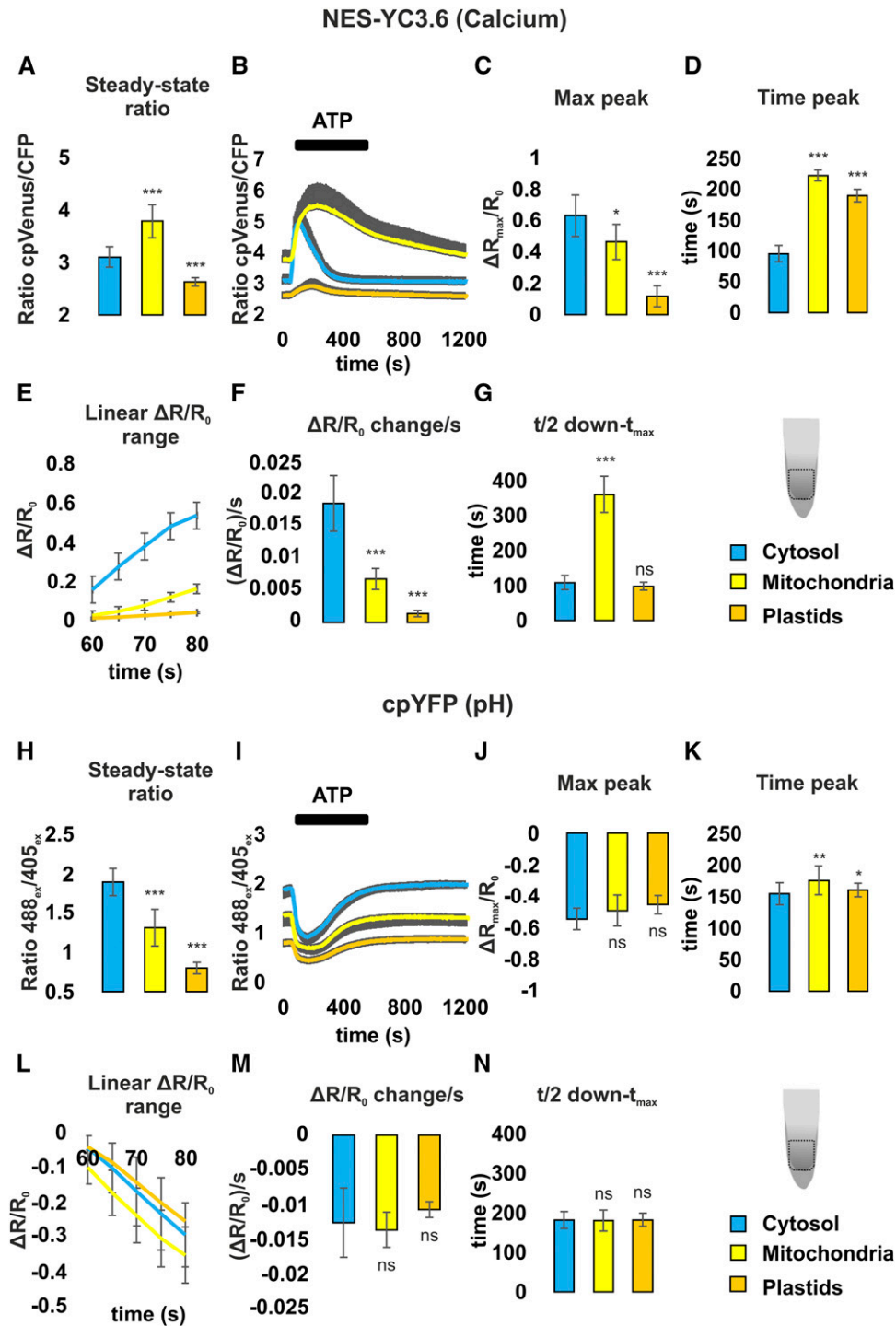


Figure 4. Ca²⁺ and pH Transients Are Linked in the Cytosol, but This Link Is Modulated in Mitochondria and Plastids of Seedling Root Tip Cells.

(A) Steady-state cpVenus/CFP ratios preceding ATP administration (averaged over 50-s time window).
 (B) Root tips of seedlings expressing NES-YC3.6 in wild type (turquoise), 4mt-YC3.6 (yellow), and 2Bam4-YC3.6 (orange) imaged under continuous perfusion and treated with 0.1 mM ATP for 3 min. cpVenus/CFP ratios of the ROI shown in the inset (schematic drawing) are plotted over time.
 (C) Peak cpVenus/CFP ratios as $\Delta R/R_0$ maximum increase after ATP administration.
 (D) Time when $\Delta R_{max}/R_0$ increase after ATP administration is reached.
 (E) cpVenus/CFP ratio expressed as $\Delta R/R_0$ increase following ATP administration; linear region was selected with $R^2 > 0.985$.
 (F) Linear rate representing slope of regression of (E).

opposite is true for pH-GFP; Supplemental Figures 1A to 1D). The analyses of the cpYFP resting ratios in the three different pH sensor lines showed differential steady states (Figure 4H), but all three subcellular localizations showed a common steep pH drop with similar kinetics at ATP treatment (Figure 4I). Ratio normalization showed that the maximum ratio changes were not statistically different between the different compartments (Figure 4J), occurring almost simultaneously even if, in both mitochondria and plastids, the peak was slightly delayed when compared with the cytosol (155 ± 18 s for cytosol; 176 ± 23 s for mitochondria and 160 ± 11 s for plastids) (Figure 4K). This delay was much smaller than the nearly 100-s delay for reaching the maximum Ca²⁺ accumulation in mitochondria and plastids compared with the cytosol (Figure 4D). Both the speed of the pH decrease (Figures 4L and 4M) and the time of recovery (Figure 4N) were almost identical between the three cell compartments. No significant differences were observed, indicating that the pH dynamics were practically identical among the compartments, in contrast with the Ca²⁺ dynamics (Supplemental Figure 4). This difference appears particularly remarkable because it suggests integration, as opposed to simple equilibration, at the boundary membranes of both the mitochondria and the plastids, which shape their internal Ca²⁺ dynamics through specific regulation of uptake, buffering, and export. The mitochondrial calcium uniporter has recently been found to offer such integration by mediating Ca²⁺-regulated Ca²⁺ uptake (recently discussed in Wagner et al., 2016). By contrast, there is little difference in the matrix and stromal pH dynamics, hinting at simple pH coupling across compartments, for example, via proton-coupled transporters, that keep pH gradients across the organelle membranes unchanged. The pH drop in the plastid likely influences stromal physiology. In chloroplasts, pH is a central determinant of photosynthetic regulation and recently also Ca²⁺ regulation has been observed at several levels of chloroplast function (Nomura and Shiina, 2014; Hochmal et al., 2016; Frank et al., 2018). Organelle-specific effects on the technical sensor behavior cannot be completely ruled out as potential contributors to the observed differences, even when the same protein sensor is used (here YC3.6 for Ca²⁺ and cpYFP for pH).

DISCUSSION

In this study, we show that Ca²⁺ and pH dynamics are linked in the cytosol of plant cells subjected to external challenges (Figure 1). Our data suggest that the cytosolic pH is linked to a stimulus-induced change of [Ca²⁺]_{cyt} and that pH changes can show different dynamics in response to different stimuli. Our observations

generalize previous reports and theoretical considerations and support the concept of a pH signature that may encode additional information to the Ca²⁺ signature and may be decoded by different downstream responders (reviewed in Felle, 2001).

Given the magnitude of the acidification, which can be estimated to be between 0.1 and 0.25 pH units in response to NAA, wounding, and ATP (based on our in vivo calibration of the pH-GFP sensor; Supplemental Figures 1A to C), the observed pH dynamics are likely to have direct physiological significance. The estimated values are in agreement with pH changes measured in HeLa cells in response to histamine (0.12 pH units; Poburko et al., 2011), with the spontaneous pH oscillations observed in the alkaline band of growing pollen tubes (magnitudes ranging from 0.3 to 0.5 pH units; Feijó et al., 2001), in guard cells in response to ABA or IAA (Irving et al., 1992; Blatt and Armstrong, 1993), and in Arabidopsis root epidermal cells in response to mechanical stimulation (Monshausen et al., 2009). pH changes of this size likely affect a multitude of downstream functions through the protonation of residues with a pK_a around the steady-state pH_{cyt} as well as on proton gradients affecting transport and energy status. For instance, PM H⁺-ATPase activity in microsomal fractions from Arabidopsis seedlings showed a stimulation by 50% in response to a pH shift from 7.2 to 6.9 (De Michelis and Spanswick, 1986; Supplemental Figure 7). Elegant work in *Caenorhabditis elegans* even established H⁺ as bona fide neurotransmitters in muscle contraction, exemplifying the central regulatory role that pH changes can play (Beg et al., 2008). A particularly striking example for intracellular pH regulation in plant cells is provided by the external mitochondrial NAD(P)H DEHYDROGENASE B1, which contributes to the alternative respiratory pathway and was shown to be stimulated by increases in [Ca²⁺]_{cyt}. However, biochemical data revealed that the enzyme is only sensitized to Ca²⁺ regulation by a coincident decrease of pH (Hao et al., 2015). Our data now reveal that, in vivo, those changes coincide, providing the physiological basis for active regulation of the NADPH oxidation pathway to occur. Similar mechanisms are likely for other prominent players in Ca²⁺ signaling, such as kinases and phosphatases (reviewed in Felle, 2001) and our work offers a physiological framework for targeted future investigation.

Employing a carefully optimized system of fluorescent protein biosensors, we were able to refine and generalize the already available evidence of linkage between [Ca²⁺]_{cyt} and pH_{cyt} dynamics in plant cells. Despite much effort, we did not find a way to perturb the [Ca²⁺]_{cyt} and pH_{cyt} link. This may be either because we have not included a critical candidate or because the linkage is the result of a larger range of mechanisms. This evidence allows

Figure 4. (continued).

(G) Time to pass half-maximal ratio during recovery.

(H) Steady-state 488_{ex}/405_{ex} ratios preceding ATP application (averaged over 50-s time window).

(I) Root tips of seedlings expressing C-cpYFP in the cytosol (turquoise), MT-cpYFP in the mitochondria (yellow), and TKTP-cpYFP (orange) imaged under continuous perfusion and treated with 0.1 mM ATP for 3 min. 488_{ex}/405_{ex} ratios of the ROI shown in the inset (schematic drawing) are plotted over time.

(J) Peak 488_{ex}/405_{ex} ratios as $\Delta R/R_0$ maximum decrease after ATP administration.

(K) Time when $\Delta R_{\max}/R_0$ decrease after ATP administration is reached.

(L) 488_{ex}/405_{ex} ratio expressed as $\Delta R/R_0$ decrease following ATP administration; linear region was selected with $R^2 > 0.995$.

(M) Linear rate representing slope of regression of **(L)**.

(N) Time to pass half-maximal ratio during recovery. $n \geq 7$; * $P \leq 0.05$, ** $P \leq 0.01$, and *** $P \leq 0.001$ (t test); error bars = sd.

several considerations about possible contributors. $[Ca^{2+}]_{cyt}/pH_{cyt}$ linkage by H^+ -coupled membrane transport of Ca^{2+} provides an hypothetical scenario. Ca^{2+} ATPases and Ca^{2+} exchangers, such as CAXs, export Ca^{2+} from the cytosol primarily to the apoplast and the vacuole (Bonza and De Michelis, 2011; Pittman and Hirschi, 2016), aided by the inward-facing proton gradient (Felle, 2001). The higher the rate of Ca^{2+} pumping, the higher is also the rate of H^+ entry into the cytosol. Our data that demonstrate the general linkage are consistent with this concept. Reduced Ca^{2+} influx into the cytosol, as achieved through pharmacological treatment (e.g., EGTA), coincides with reduced acidification of the cytosol (Figures 2A to 2H), possibly reflecting a reduced H^+ influx rate because of a reduced Ca^{2+} extrusion. When genetic disruption of the $[Ca^{2+}]_{cyt}/pH_{cyt}$ link was attempted, any change in $[Ca^{2+}]_{cyt}$ coincided with a change in pH_{cyt} (*aca8 aca10*). Consistently, the absence of a change in $[Ca^{2+}]_{cyt}$ came with an absence of a change in pH_{cyt} (*aca4 aca11*).

If we assume that the link between Ca^{2+} and H^+ is dependent on the activity of transporters, we can estimate the number of transported Ca^{2+} ions and protons. The change in $[Ca^{2+}]_{cyt}$ in root tip cells in response to auxin and ATP was recently estimated to reach ~ 100 – 200 nM (Waadt et al., 2017) as averaged over cells and tissues (~ 20 – 160 nM from our estimations reported in Supplemental Figure 8). It has been estimated that approximately 100 Ca^{2+} ions are bound to internal buffers for every free Ca^{2+} ion (Falcke, 2004). Hence, the removal of ~ 20 μM Ca^{2+} (specifically, 20 μ mole from every liter of cytosol) is required to bring a $\Delta[Ca^{2+}]_{cyt}$ of 200 nM back to baseline. Assuming that the Ca^{2+} ATPases or CAXs operate at a Ca^{2+}/H^+ stoichiometry of 1:2 and 1:3, respectively (Blackford et al., 1990; Carafoli, 1991), this implies that an amount corresponding to 40–60 μM of H^+ will be transported into the cytosol. For a cytosolic buffering capacity of approximately 30 mM per unit pH change (Sanders and Slayman, 1982; Bethmann and Schönknecht, 2009), this results in a pH change of 0.0013–0.00195. Even using estimates of bound/free Ca^{2+} ratio of 1700 (Fleet et al., 1998), which results in a pH change of 0.023, those values are too small (a factor of 10) to explain the observed shifts of 0.1–0.25 pH units and would not be reliably picked up in vivo by the pH sensors used in this work (Moseyko and Feldman, 2001; Schwarzländer et al., 2011, 2012, 2014) that would require 400–600 μM of H^+ .

A second candidate mechanism to underpin the Ca^{2+}/H^+ link is a buffer exchange model in which Ca^{2+} and H^+ are competing for the same binding sites of a common cytosolic buffer (Plieth et al., 1997). Although the model of Plieth et al. (1997) would explain the magnitudes of our observations, this model has been criticized for assuming an unrealistically high buffering capacity for Ca^{2+} (Schönknecht and Bethmann, 1998).

Both direct linkage models (via transporters and buffers) give rise to a one-to-one mapping between $[Ca^{2+}]_{cyt}$ and pH_{cyt} , that is, a given level of $[Ca^{2+}]_{cyt}$ leads to a well-defined pH_{cyt} and pH_{cyt} thus strictly follows every change in $[Ca^{2+}]_{cyt}$. However, the detailed dynamics of both ions, although similar, clearly differed (Figures 1A and 1E). This suggests that additional mechanisms operate on top of any direct linkage to generate flexibility between both parameters.

The observation that pH changes are rapidly passed on among cytosol, mitochondria, and plastids showing a similar signature

despite Ca^{2+} dynamics that differ between the compartments (Figure 4) is further evidence against a direct linkage model. Here, a potential modifier of the linkage may be differing buffering capacities for Ca^{2+} and H^+ in different cell compartments. Technically, it also cannot be completely ruled out that sensor response characteristics differ slightly between compartments, which may impact the signal (Granqvist et al., 2012). These considerations suggest that the $[Ca^{2+}]$ and pH link depends on further mechanisms in addition to the direct Ca^{2+}/H^+ coupled transport operated by the transporters located at different membranes, the contribution of cytosolic Ca^{2+} and pH buffers, or H^+ -pump activities (which are intrinsically dependent on $[H^+]$).

In conclusion, our study demonstrates a linkage between Ca^{2+} and H^+ in plant cells, which becomes evident by synchronous dynamics in response to different external stimuli. Those findings generalize previous observations in specialized cell structures, such as guard cells (Irving et al., 1992; Blatt and Grabov, 1997) root epidermal cells (Monshausen et al., 2009), root hairs and pollen tubes (Herrmann and Felle, 1995; Monshausen et al., 2008; Michard et al., 2011, 2017), and imply that concentration changes in both Ca^{2+} and H^+ may act in tandem in the same or even separate signal transduction events. As such, Ca^{2+} -based signaling would be best assessed by measuring the concerted dynamics of several parameters, including pH by multiparametric in vivo sensing (as recently suggested by De Col et al., 2017; Waadt et al., 2017). Capturing a more complete picture of the Ca^{2+} -linked dynamics in subcellular physiology will pave the way to understanding Ca^{2+} signaling as part of the context that it operates in, while potentially providing insights into how specificity is achieved.

METHODS

Plant Material and Growth Conditions

All *Arabidopsis thaliana* (*Arabidopsis*) plants were of the ecotype Columbia 0 (Col-0). Plants were grown on soil under short day conditions (12 h light / 12 h dark, 100 $\mu E m^{-2} s^{-1}$ of Cool White Neon lamps) at 22°C and 75% relative humidity. Seeds were surface-sterilized by vapor-phase sterilization (Clough and Bent, 1998) and plated on half-strength Murashige and Skoog (MS) medium (Murashige and Skoog, 1962) (Duchefa) supplemented with 0.1% SUC and 0.05% MES, pH 5.8, and 0.8% plant agar (Duchefa). After stratification at 4°C in the dark for 2 d, plates were transferred to the growth chamber under long day conditions (16 h light / 8 h dark, 100 $\mu E m^{-2} s^{-1}$ of Cool White Neon lamps) at 22°C. The plates were kept vertically and seedlings were used for imaging 6–7 d after germination. *Arabidopsis* Col-0 wild-type and *rdr6* lines pGPTVII Ubq10:NES-YC3.6 (cytosolic Ca^{2+} sensor), pUpHTKan Ubq10:pH-GFP (cytoplasmic pH sensor), pH2GW7 CaMV35S:MT-cpYFP (mitochondrial pH sensor), pGreen0179 CaMV35S:4mt-YC3.6 (mitochondrial Ca^{2+} sensor), and *rdr6* pGreen0029 CaMV35S:2Bam4-YC3.6 (plastidial Ca^{2+} sensor) were previously reported (Schwarzländer et al., 2011, 2012; Krebs et al., 2012; Loro et al., 2012, 2016; Fendrych et al., 2014).

Molecular Cloning and Plasmid Constructs

The core coding sequence of cpYFP was PCR-amplified from a MT-cpYFP insert in a pShuttle-CMV vector (Wang et al., 2008) using extension primers for cloning using Gateway technology (Invitrogen). For cytosolic localization, the product was first inserted into a pDONR207 vector (Invitrogen)

and then transferred into a pH2GW7 vector (Karimi et al., 2002) under the control of the CaMV35S promoter. For sensor localization in the plastid stroma, the sequence of the *Nicotiana tabacum* chloroplast transit peptide (TKTP) (Wirtz and Hell, 2003; Schwarzländer et al., 2008) was fused in-frame to the cpYFP sequence by PCR using primer extension. Primer sequences are detailed in Supplemental Table 1. Correctness of the sequences was confirmed by commercial sequencing.

Generation of Transgenic Plants

Plant transformation was performed using *Agrobacterium tumefaciens* GV3101 cells by floral-dip (Clough and Bent, 1998). Per construct, several independent transgenic lines were selected by antibiotic resistance or presence of fluorescence. pGPTVII Ubq10:NES-YC3.6 and pUpHTKan Ubq10:pH-GFP constructs were introduced in the double knock-out *aca8 aca10* and *aca4 aca11* Arabidopsis T-DNA line reported in Freidit Frey et al. (2012) and Boursiac et al. (2010), respectively. The C-cpYFP and TKTP-cpYFP constructs were introduced in Col-0 wild-type plants and transformants were selected by hygromycin resistance and YFP fluorescence, and the same markers were also used for segregation analysis to select for homozygous lines.

Confocal Laser Scanning Microscopy

Confocal laser scanning microscopy analyses were performed using a Leica SP2 imaging system. cpYFP and chlorophyll were excited by the 488-nm line of the argon laser and the emission was collected at 525–540 nm and 650–750 nm, respectively. Images were acquired by a 40× oil immersion objective with different digital zooms. Images were analyzed using FIJI software.

Fluorescence Microscopy

For Ca²⁺ and pH imaging analyses, an inverted fluorescence microscope (Ti-E; Nikon) with a CFI 4× numerical aperture 0.13 dry objective for entire leaves or a 20× numerical aperture 0.75 for seedling roots were used. Excitation light was produced by a fluorescent lamp (Prior Lumen 200 PRO; Prior Scientific) set to 20% (for roots) and 50% (for leaves) with 440 nm (436/20 nm) for the Cameleon (YC3.6) sensor or 405 nm (405/40 nm) and 488 nm (470/40 nm) for pH-GFP and cpYFP sensors. Images were collected with a dual charge-coupled device camera (ORCA-D2; Hamamatsu). For Cameleon analysis, the Förster resonance energy transfer CFP/YFP optical block A11400-03 (emission 1, 483/32 nm for CFP; emission 2, 542/27 nm for Förster resonance energy transfer) with a dichroic 510-nm mirror (Hamamatsu) was used for the simultaneous CFP and cpVenus acquisitions. For pH-GFP and cpYFP imaging, the emissions were collected using a 505/530-nm bandpass filter (Chroma Technology) with both excitation wavelengths (405 and 488 nm) used sequentially to illuminate the sample. Camera binning (2 × 2 or 4 × 4) and exposure times (from 50 to 400 ms) were adjusted depending on the sensor line and analyzed tissue. Images were acquired every 2 s for leaves and 5 s for roots. Filters and the dichroic mirrors were purchased from Chroma Technology. NIS-Elements (Nikon) was used as a platform to control the microscope, illuminator, and camera. Images were analyzed using FIJI.

Seedling and Leaf Imaging

Seven-d-old seedlings were used for root imaging. Seedlings were kept in the growth chamber until the experiment. For root experiments, the seedlings were gently removed from the plate according to Behera and Kudla (2013), placed in the dedicated chambers, and overlaid with cotton wool soaked in imaging solution (5 mM KCl, 10 mM MES, and 10 mM CaCl₂, pH 5.8 adjusted with Tris-base). The root was continuously perfused with

imaging solution whereas the shoot was not submerged. Treatments were performed by supplementing the imaging solution with 0.1 mM sodium adenosine triphosphate (Na₂ATP, from a 200 mM stock solution buffered at pH 7.4 with NaOH) or 0.01 mM NAA (from a 10.74 mM stock solution) and administered for 3 min under running perfusion.

To perform the experiments reported in Figures 2A and 2B in which the extracellular Ca²⁺ was chelated, a modified imaging solution was used (5 mM KCl, 10 mM MES, 50 μM CaCl₂, and 1 mM EGTA, pH 5.8 adjusted with Tris-base). For chemical treatments, seedlings were pre-incubated for 10 min in 5 cm petri dishes in the imaging solution supplemented with 5 μM Nigericin or 5 μM FCCP. Solvent control seedlings were kept for the same times in the imaging solution supplemented with 0.1% (v/v) EtOH. Seedlings were then transferred to the imaging chamber under running perfusion and allowed to recover for ~10 min before measurement. It should be noted that the resting Ca²⁺ ratios of the NES-YC3.6 seedlings in Figure 2 are lower than those reported in Figures 3 and 4 even if the microscope settings were the same. Consistently, the experiments conducted using wild-type and mutant seedlings or control and treated seedlings were performed side by side. Hence, every single imaging experiment has its internal control. Wounding of leaves from 6-week-old Arabidopsis plants was performed by gently pressing the lamina with laboratory forceps as described in Costa et al. (2017).

Quantitative Imaging Analysis

Fluorescence intensity was determined over regions of interest (ROIs), which corresponded to the cells surrounding the wounded region, or the root tip meristematic or transition zones. The cpVenus and CFP emissions, pH-GFP and cpYFP 405 and 488 emissions of the analyzed ROIs, were used for the ratio (*R*) calculations (cpVenus/CFP; 405_{ex}/488_{ex}; 488_{ex}/405_{ex}) and, where suitable, normalized to the initial ratio (*R*₀) and plotted versus time ($\Delta R/R_0$). Background subtraction was performed independently for both channels before calculating the ratio.

In vivo and Semi in vivo pH-GFP and C-cpYFP Sensor Calibrations

For the pH-GFP and C-cpYFP sensors calibration, two different methods were adopted. The first protocol was based on the same perfusion system used for the seedling root imaging experiments. Specifically, seedlings were perfused with the following solutions: 1) 50 mM MES-BTP pH 6.0, 50 mM CH₃COONH₄; 2) 50 mM MES-BTP pH 6.5, 50 mM CH₃COONH₄; 3) 50 mM MES-BTP pH 6.75, 50 mM CH₃COONH₄; 4) 50 mM HEPES-BTP pH 7.0, 50 mM CH₃COONH₄; 5) 50 mM HEPES-BTP pH 7.5, 50 mM CH₃COONH₄; and 6) 50 mM HEPES-BTP pH 8.0, 50 mM CH₃COONH₄. The solutions at different values of pH were exchanged every 5 min for seedlings expressing the C-cpYFP sensor or 10 min for those expressing the pH-GFP sensor.

The in vivo pH-GFP response linearity ($R^2 = 0.9908$), measured as $\Delta R/R_0$ variations in response to the treatment with different external pH buffers (from pH 6.0 with a $\Delta R/R_0 = 0$ to pH 8.0 with $\Delta R/R_0 = 1.49$; Supplemental Figure 1A to S1C), allowed estimation of the pH unit variations observed in response to the different stimuli reported in Figure 1. Making the rough assumption that the degree of change occurring for internal and external pH was the same (i.e., constant pH gradient across the plasma membrane and change within the linear range of the pH sensor), the following cytosolic pH variations in response to the different stimuli can be estimated: wounding 0.257 units, ATP 0.268 units, and NAA 0.121 units.

The second protocol was adapted from Wagner et al. (2015b). Seedlings expressing both pH-GFP and C-cpYFP sensors were individually submerged, for 15 min, in buffer solutions adjusted at different pHs (6, 7, and 8) and in presence of 5 μM of FCCP that, being able to transport protons through cell membranes, can equilibrate the internal (cytoplasmic) and external (medium) pHs. The solutions were the following: 1) 100 mM

MES-Tris, 40 mM K_2SO_4 , 5 μ M FCCP, and $0.5 \times$ MS salt, pH 6.0; 2) 100 mM MOPS-Tris, 40 mM K_2SO_4 , 5 μ M FCCP, and $0.5 \times$ MS salt, pH 7.0; and 3) 100 mM HEPES-Tris, 40 mM K_2SO_4 , 5 μ M FCCP, and $0.5 \times$ MS salt, pH 8.0. Seedlings were then mounted on a microscope slide and imaged for 1 min as described above. This second semi in vivo protocol showed a reduced response of both sensors compared with the in vivo calibration. However, in agreement with the first protocol, the pH-GFP response shows again a clear linearity in the tested pH range, whereas the C-cpYFP sensor confirmed, as previously reported (Schwarzländer et al., 2011, 2014), a higher sensitivity for more alkaline pHs.

Microsomal Membrane Isolation

Ten-d-old seedlings (~5 g) were homogenized as reported in Cerana et al. (2006). The homogenate was centrifuged at 2000g at 4°C for 12 min and the resulting supernatant was centrifuged at 20,000g at 4°C for 1 h. Pellet, containing microsomal membranes, was washed and resuspended as previously described in Cerana et al. (2006). Protein concentration was determined using the Bradford assay reagent (Bio-Rad).

pH-Dependence of the Activation of Arabidopsis PM H⁺-ATPase in Microsomal Membrane Fractions

Vanadate-sensitive hydrolytic activity of PM H⁺-ATPase was assayed as reported in Viotti et al. (2005) at the specified pHs to mimic the cytosol acidification. Released Pi was determined as described in De Michelis and Spanswick (1986). Results are from one experiment with three technical replicates, representative of three giving similar results.

Statistical Analysis

All the data are representative of at least ≥ 3 experiments. Reported traces are averages of traces from all single experiments used for the statistical analyses. Results are reported as averages \pm SDs. The $(\Delta R/R_0)/s$ ratio changes were calculated in the linear range ($R^2 \geq 0.98$) of Ca²⁺ increase or pH decrease, respectively. The *P* values were calculated with an unpaired Student's *t* test. Statistical significance was also validated using one-way analysis of variance and with post hoc Tukey Honestly Significant Difference tests.

ACCESSION NUMBERS

Sequence data for ACA8 (At5g57110), ACA10 (At4g29900), ACA4 (At2g41560), and ACA11 (At3g57330) can be found in the Arabidopsis Araport (<https://www.araport.org/>) or TAIR (<https://www.arabidopsis.org/>) databases.

SUPPLEMENTAL DATA

Supplemental Figure 1. In vivo and semi in vivo responses of cytosolic localized pH-GFP and C-cpYFP sensors.

Supplemental Figure 2. Superimposition of averaged cpVenus/CFP and 405_{ex}/488_{ex} ratio traces of wild type and *aca8 aca10* mutant shown in Figure 3.

Supplemental Figure 3. Genetic ablation of ACA4 and ACA11 Ca²⁺-ATPase does not affect either Ca²⁺ and pH cytosolic transients induced by external ATP.

Supplemental Figure 4. Superimposition of averaged cpVenus/CFP and 488_{ex}/405_{ex} ratio traces of cytosol, mitochondria and plastids shown in Figure 4.

Supplemental Figure 5. Arabidopsis Col-0 transgenic seedlings expressing the cpYFP sensor localized to different subcellular compartments.

Supplemental Figure 6. Comparison of cpYFP subcellular localization in cotyledon leaf cells of the C-cpYFP, MT-cpYFP and TKTP-cpYFP transgenic lines.

Supplemental Figure 7. pH-dependence of the activation of Arabidopsis plasma membrane H⁺-ATPase in microsomal membranes.

Supplemental Figure 8. NES-YC3.6 calibration in Arabidopsis root tip cells.

Supplemental Table 1. Primer sequences for the cpYFP constructs generation.

Supplemental Movie 1. Ratiometric cpVenus/CFP false-color (LUT: Fire) movie from a representative time series of a wild-type Arabidopsis leaf expressing the NES-YC3.6 sensor in response to wounding.

Supplemental Movie 2. Ratiometric 405_{ex}/488_{ex} false-color (LUT: Green Fire Blue) movie from a representative time series of a wild-type Arabidopsis leaf expressing the pH-GFP sensor in response to wounding.

Supplemental Movie 3. Movie from a representative time series of a wild-type Arabidopsis seedling root tip expressing the pH-GFP sensor perfused with solutions adjusted to different pHs.

Supplemental Movie 4. Ratiometric cpVenus/CFP false-color (LUT: Fire) movie from a representative time series of a wild-type Arabidopsis seedling root tip expressing the NES-YC3.6 sensor in response to external ATP.

Supplemental Movie 5. Ratiometric 405_{ex}/488_{ex} false-color (LUT: Green Fire Blue) movie from a representative time series of a wild-type Arabidopsis seedling root tip expressing the pH-GFP sensor in response to external ATP.

Supplemental Movie 6. Ratiometric cpVenus/CFP false-color (LUT: Fire) movie from a representative time series of a wild-type Arabidopsis seedling root tip expressing the NES-YC3.6 sensor in response to NAA.

Supplemental Movie 7. Ratiometric 405_{ex}/488_{ex} false-color (LUT: Green Fire Blue) movie from a representative time series of a wild-type Arabidopsis seedling root tip expressing the pH-GFP sensor in response to NAA.

Supplemental Movie 8. Movie from a representative time series of wild-type Arabidopsis seedling root tip cells expressing the C-cpYFP sensor perfused with solutions adjusted to different pH values.

Supplemental Movie Legends.

ACKNOWLEDGMENTS

The *aca8 aca10* mutant line was kindly provided by Silke Robatzek (The Sainsbury Laboratory, Norwich Research Park, Norwich, UK). The *aca4 aca11* mutant line was kindly provided by Jeff Harper (University of Nevada, Reno). The pH-GFP Arabidopsis line and plasmid were kindly provided by Dr. Melanie Krebs (University of Heidelberg, Germany), who also provided the in vivo pH-GFP calibration protocol. The authors thank Stephan Wagner for discussions about quantitative data analysis and the drawings in Supplemental Figure 4.

The authors are grateful to five anonymous reviewers whose constructive critique, comments and suggestions greatly improved the manuscript.

This work was supported by the Ministero dell'Istruzione, dell'Università e della Ricerca Fondo per gli Investimenti della Ricerca di Base (FIRB)2010 RBF10S1LJ_001 grant to A.C. and by PIANO DI SVILUPPO DI ATENEO 2016 (Università degli Studi di Milano) to A.C. Z.X. thanks the National Natural Science Foundation of China (31701454). M.S. thanks the Deutsche Forschungsgemeinschaft for funding through the Emmy-Noether Program (SCHW1719/ 1-1), the Research Training Group GRK2064, and a grant (SCHW1719/5-1) as part of the package PAK918. R.J.M. acknowledges support from BBSRC's Institute Strategic Program on Biotic Interactions underpinning Crop Productivity (BB/J004553/1) and Plant Health (BB/P012574/1).

AUTHOR CONTRIBUTIONS

A.C., M.C.B., and M.I.D.M. designed the research. A.C. directed the research. L.L. and M.C.B. generated the knock-out mutant lines expressing the NES-YC3.6 and pH-GFP sensors. M.S. generated the cpYFP sensor lines. S.B., X.Z., F.G.D., and A.C. performed the imaging experiments. A.C. analyzed the data and generated all figures and supplemental material. R.J.M. estimated the expected pH and Ca²⁺ responses based on known buffering capacities. A.C., R.J.M., and M.S. wrote the article. M.I.D.M. revised the article.

Received August 28, 2018; accepted October 29, 2018; published October 29, 2018.

REFERENCES

- Armbruster, U., Correa Galvis, V., Kunz, H.H., and Strand, D.D.** (2017). The regulation of the chloroplast proton motive force plays a key role for photosynthesis in fluctuating light. *Curr. Opin. Plant Biol.* **37**: 56–62.
- Barbez, E., Dünser, K., Gaidora, A., Lendl, T., and Busch, W.** (2017). Auxin steers root cell expansion via apoplastic pH regulation in *Arabidopsis thaliana*. *Proc. Natl. Acad. Sci. USA* **114**: E4884–E4893.
- Beffagna, N., Romani, G., and Sforza, M.C.** (2000). H⁺ fluxes at plasmalemma level: In vivo evidence for a significant contribution of the Ca²⁺-ATPase and for the involvement of its activity in the abscisic acid-induced changes in *Egeria densa* leaves. *Plant Biol.* **2**: 168–175.
- Beg, A.A., Ernstrom, G.G., Nix, P., Davis, M.W., and Jorgensen, E. M.** (2008). Protons act as a transmitter for muscle contraction in *C. elegans*. *Cell* **132**: 149–160.
- Behera, S., and Kudla, J.** (2013). High-resolution imaging of cytoplasmic Ca²⁺ dynamics in Arabidopsis roots. *Cold Spring Harb. Protoc.* **2013**: 665–669.
- Beneloujaephajri, E., Costa, A., L'Haridon, F., Métraux, J.P., and Binda, M.** (2013). Production of reactive oxygen species and wound-induced resistance in *Arabidopsis thaliana* against Botrytis cinerea are preceded and depend on a burst of calcium. *BMC Plant Biol.* **13**: 160.
- Bethmann, B., and Schönknecht, G.** (2009). pH regulation in an acidophilic green alga—A quantitative analysis. *New Phytol.* **183**: 327–339.
- Blackford, S., Rea, P.A., and Sanders, D.** (1990). Voltage sensitivity of H⁺/Ca²⁺ antiport in higher plant tonoplast suggests a role in vacuolar calcium accumulation. *J. Biol. Chem.* **265**: 9617–9620.
- Blatt, M.R., and Armstrong, F.** (1993). K⁺ channels of stomatal guard cells: Abscisic-acid-evoked control of the outward rectifier mediated by cytoplasmic pH. *Planta* **191**: 330–341.
- Blatt, M.R., and Grabov, A.** (1997). Signal redundancy, gates and integration in the control of ion channels for stomatal movement. *J. Exp. Bot.* **48**: 529–537.
- Bonza, M.C., and De Michelis, M.I.** (2011). The plant Ca²⁺-ATPase repertoire: Biochemical features and physiological functions. *Plant Biol (Stuttg)* **13**: 421–430.
- Bonza, M.C., Loro, G., Behera, S., Wong, A., Kudla, J., and Costa, A.** (2013). Analyses of Ca²⁺ accumulation and dynamics in the endoplasmic reticulum of Arabidopsis root cells using a genetically encoded Cameleon sensor. *Plant Physiol.* **163**: 1230–1241.
- Boursiac, Y., Lee, S.M., Romanowsky, S., Blank, R., Sladek, C., Chung, W.S., and Harper, J.F.** (2010). Disruption of the vacuolar calcium-ATPases in Arabidopsis results in the activation of a salicylic acid-dependent programmed cell death pathway. *Plant Physiol.* **154**: 1158–1171.
- Brini, M., and Carafoli, E.** (2009). Calcium pumps in health and disease. *Physiol. Rev.* **89**: 1341–1378.
- Cao, Y., Tanaka, K., Nguyen, C.T., and Stacey, G.** (2014). Extracellular ATP is a central signaling molecule in plant stress responses. *Curr. Opin. Plant Biol.* **20**: 82–87.
- Carafoli, E.** (1991). Calcium pump of the plasma membrane. *Physiol. Rev.* **71**: 129–153.
- Carraretto, L., Teardo, E., Checchetto, V., Finazzi, G., Uozumi, N., and Szabo, I.** (2016). Ion channels in plant bioenergetic organelles, chloroplasts and mitochondria: from molecular identification to function. *Mol. Plant* **9**: 371–395.
- Cerana, M., Bonza, M.C., Harris, R., Sanders, D., and De Michelis, M.I.** (2006). Abscisic acid stimulates the expression of two isoforms of plasma membrane Ca²⁺-ATPase in *Arabidopsis thaliana* seedlings. *Plant Biol (Stuttg)* **8**: 572–578.
- Choi, J., Tanaka, K., Cao, Y., Qi, Y., Qiu, J., Liang, Y., Lee, S.Y., and Stacey, G.** (2014). Identification of a plant receptor for extracellular ATP. *Science* **343**: 290–294.
- Clapham, D.E.** (2007). Calcium signaling. *Cell* **131**: 1047–1058.
- Clough, S.J., and Bent, A.F.** (1998). Floral dip: A simplified method for *Agrobacterium*-mediated transformation of *Arabidopsis thaliana*. *Plant J.* **16**: 735–743.
- Costa, A., Luoni, L., Marrano, C.A., Hashimoto, K., Köster, P., Giacometti, S., De Michelis, M.I., Kudla, J., and Bonza, M.C.** (2017). Ca²⁺-dependent phosphoregulation of the plasma membrane Ca²⁺-ATPase ACA8 modulates stimulus-induced calcium signatures. *J. Exp. Bot.* **68**: 3215–3230.
- Costa, A., Navazio, L., and Szabo, I.** (2018). The contribution of organelles to plant intracellular calcium signalling. *J. Exp. Bot.* **69**: 4175–4193.
- De Col, V., Fuchs, P., Nietzel, T., Elsässer, M., Voon, C.P., Candeo, A., Seeliger, I., Fricker, M.D., Grefen, C., Möller, I.M., Bassi, A., and Lim, B.L., et al.** (2017) ATP sensing in living plant cells reveals tissue gradients and stress dynamics of energy physiology. *Elife*.
- De Michelis, M.I., and Spanswick, R.M.** (1986). H-pumping driven by the vanadate-sensitive ATPase in membrane vesicles from corn roots. *Plant Physiol.* **81**: 542–547.
- De Vriese, K., Costa, A., Beeckman, T., and Vanneste, S.** (2018). Pharmacological strategies for manipulating plant Ca²⁺ signalling. *Int J Mol Sci.*
- Dindas, J., Scherzer, S., Roelfsema, M.R.G., von Meyer, K., Müller, H.M., Al-Rasheid, K.A.S., Palme K., Dietrich, P., Becker, D., Bennett, M.J., and Hedrich, R.** (2018). AUX1-mediated root hair auxin influx governs SCF^{TIR1/AFB}-type Ca²⁺ signaling. *Nat Commun.* **9**: 1174.
- Dodd, A.N., Kudla, J., and Sanders, D.** (2010). The language of calcium signaling. *Annu. Rev. Plant Biol.* **61**: 593–620.

- Duby, G., and Boutry, M. (2009). The plant plasma membrane proton pump ATPase: A highly regulated P-type ATPase with multiple physiological roles. *Pflügers Arch.* **457**: 645–655.
- Emery, L., Whelan, S., Hirschi, K.D., and Pittman, J.K. (2012). Protein phylogenetic analysis of Ca²⁺/cation antiporters and insights into their evolution in plants. *Front. Plant. Sci.* **3**: 1.
- Falcke, M. (2004). Reading the patterns in living cells—The physics of Ca²⁺ signaling. *Adv. Phys.* **53**: 255–440.
- Feijó, J.A., Sainhas, J., Holdaway-Clarke, T., Cordeiro, M.S., Kunkel, J.G., and Hepler, P.K. (2001). Cellular oscillations and the regulation of growth: The pollen tube paradigm. *BioEssays* **23**: 86–94.
- Felle, H.H. (2001). pH: Signal and messenger in plant cells. *Plant Biol.* **3**: 577–591.
- Fendrych, M., Van Hautegeem, T., Van Durme, M., Olvera-Carrillo, Y., Huysmans, M., Karimi, M., Lippens, S., Guérin, C.J., Krebs, M., Schumacher, K., and Nowack, M.K. (2014). Programmed cell death controlled by ANAC033/SOMBRERO determines root cap organ size in *Arabidopsis*. *Curr. Biol.* **24**: 931–940.
- Fleet, A., Ellis-Davies, G., and Bolsover, S. (1998). Calcium buffering capacity of neuronal cell cytosol measured by flash photolysis of calcium buffer NP-EGTA. *Biochem. Biophys. Res. Commun.* **250**: 786–790.
- Frank, J., Happeck, R., Meier, B., Hoang, M.T.T., Stribny, J., Hause, G., Ding, H., Morsomme, P., Baginsky, S., and Peiter, E. (2018). Chloroplast-localized BICAT proteins shape stromal calcium signals and are required for efficient photosynthesis. *New Phytol.*
- Frei dit Frey, N., Mbengue, M., Kwaaitaal, M., Nitsch, L., Altenbach, D., Häweker, H., Lozano-Duran, R., Njo, M.F., Beeckman, T., Huettel, B., Borst, J.W., and Panstruga, R., et al. (2012) Plasma membrane calcium ATPases are important components of receptor-mediated signaling in plant immune responses and development. *Plant Physiol.* **159**: 798–809.
- Gao, D., Knight, M.R., Trewavas, A.J., Sattelmacher, B., and Plieth, C. (2004). Self-reporting *Arabidopsis* expressing pH and [Ca²⁺] indicators unveil ion dynamics in the cytoplasm and in the apoplast under abiotic stress. *Plant Physiol.* **134**: 898–908.
- Gaxiola, R.A., Palmgren, M.G., and Schumacher, K. (2007). Plant proton pumps. *FEBS Lett.* **581**: 2204–2214.
- Gjetting, K.S., Ytting, C.K., Schulz, A., and Fuglsang, A.T. (2012). Live imaging of intra- and extracellular pH in plants using pHusion, a novel genetically encoded biosensor. *J. Exp. Bot.* **63**: 3207–3218.
- Granqvist, E., Wysham, D., Hazledine, S., Kozłowski, W., Sun, J., Charpentier, M., Martins, T.V., Haleux, P., Tsaneva-Atanasova, K., Downie, J.A., Oldroyd, G.E.D., and Morris, R.J. (2012). Buffering capacity explains signal variation in symbiotic calcium oscillations. *Plant Physiol.* **160**: 2300–2310.
- Hao, M.-S., Jensen, A.M., Boquist, A.-S., Liu, Y.-J., and Rasmusson, A.G. (2015). The Ca²⁺-regulation of the mitochondrial external NADPH dehydrogenase in plants is controlled by cytosolic pH. *PLoS One* **10**: e0139224.
- Herrmann, A., and Felle, H. (1995). Tip growth in root hair cells of *Sinapis alba* L.: Significance of internal and external Ca²⁺ and pH. *New Phytol.* **129**: 523–533.
- Hille, B. (1992). *Ion Channels in Excitable Membrane*, Sinauer Associates, Sunderland, MA
- Hochmal, A.K., Zinzius, K., Charoenwattanasatien, R., Gäbelein, P., Mutoh, R., Tanaka, H., Schulze, S., Liu, G., Scholz, M., Nordhues, A., Offenborn, J.N., and Petroustos, D., et al. (2016) Calredoxin represents a novel type of calcium-dependent sensor-responder connected to redox regulation in the chloroplast. *Nat. Commun.* **7**: 11847.
- Irving, H.R., Gehring, C.A., and Parish, R.W. (1992). Changes in cytosolic pH and calcium of guard cells precede stomatal movements. *Proc. Natl. Acad. Sci. USA* **89**: 1790–1794.
- Karimi, M., Inzé, D., and Depicker, A. (2002). GATEWAY vectors for *Agrobacterium*-mediated plant transformation. *Trends Plant Sci.* **7**: 193–195.
- Krebs, M., Held, K., Binder, A., Hashimoto, K., Den Herder, G., Parniske, M., Kudla, J., and Schumacher, K. (2012). FRET-based genetically encoded sensors allow high-resolution live cell imaging of Ca²⁺ dynamics. *Plant J.* **69**: 181–192.
- Logan, D.C., and Knight, M.R. (2003). Mitochondrial and cytosolic calcium dynamics are differentially regulated in plants. *Plant Physiol.* **133**: 21–24.
- Loro, G., Drago, I., Pozzan, T., Schiavo, F.L., Zottini, M., and Costa, A. (2012). Targeting of Cameleons to various subcellular compartments reveals a strict cytoplasmic/mitochondrial Ca²⁺ handling relationship in plant cells. *Plant J.* **71**: 1–13.
- Loro, G., Wagner, S., Doccula, F.G., Behera, S., Weini, S., Kudla, J., Schwarzländer, M., Costa, A., and Zottini, M. (2016). Chloroplast-specific in vivo Ca²⁺ imaging using Yellow Cameleon Fluorescent Protein sensors reveals organelle-autonomous Ca²⁺ signatures in the stroma. *Plant Physiol.* **171**: 2317–2330.
- Luoni, L., Bonza, M.C., and De Michelis, M.I. (2000). H⁺/Ca²⁺ exchange driven by the plasma membrane Ca²⁺-ATPase of *Arabidopsis thaliana* reconstituted in proteoliposomes after calmodulin-affinity purification. *FEBS Lett.* **482**: 225–230.
- Martins, T.V., Evans, M.J., Woolfenden, H.C., and Morris, R.J. (2013). Towards the physics of calcium signalling in plants. *Plants (Basel)* **2**: 541–588.
- Michard, E., Lima, P.T., Borges, F., Silva, A.C., Portes, M.T., Carvalho, J.E., Gilliam, M., Liu, L.H., Obermeyer, G., and Feijó, J.A. (2011). Glutamate receptor-like genes form Ca²⁺ channels in pollen tubes and are regulated by pistil D-serine. *Science* **332**: 434–437.
- Michard, E., Simon, A.A., Tavares, B., Wudick, M.M., and Feijó, J.A. (2017). Signaling with ions: The keystone for apical cell growth and morphogenesis in pollen tubes. *Plant Physiol.* **173**: 91–111.
- Monshausen, G.B., Messerli, M.A., and Gilroy, S. (2008). Imaging of the Yellow Cameleon 3.6 indicator reveals that elevations in cytosolic Ca²⁺ follow oscillating increases in growth in root hairs of *Arabidopsis*. *Plant Physiol.* **147**: 1690–1698.
- Monshausen, G.B., Bibikova, T.N., Weisenseel, M.H., and Gilroy, S. (2009). Ca²⁺ regulates reactive oxygen species production and pH during mechanosensing in *Arabidopsis* roots. *Plant Cell* **21**: 2341–2356.
- Monshausen, G.B., Miller, N.D., Murphy, A.S., and Gilroy, S. (2011). Dynamics of auxin-dependent Ca²⁺ and pH signaling in root growth revealed by integrating high-resolution imaging with automated computer vision-based analysis. *Plant J.* **65**: 309–318.
- Moseyko, N., and Feldman, L.J. (2001). Expression of pH-sensitive green fluorescent protein in *Arabidopsis thaliana*. *Plant Cell Environ.* **24**: 557–563.
- Murashige, T., and Skoog, F. (1962). A revised medium for rapid growth and bioassays with tobacco tissue cultures. *Physiol. Plant.* **15**: 473–497.
- Nagai, T., Yamada, S., Tominaga, T., Ichikawa, M., and Miyawaki, A. (2004). Expanded dynamic range of fluorescent indicators for Ca²⁺ by circularly permuted yellow fluorescent proteins. *Proc. Natl. Acad. Sci. USA* **101**: 10554–10559.
- Nomura, H., and Shiina, T. (2014). Calcium signaling in plant endosymbiotic organelles: Mechanism and role in physiology. *Mol. Plant* **7**: 1094–1104.

- Pittman, J.K., and Hirschi, K.D.** (2016). CAX-ing a wide net: Cation/H⁺ transporters in metal remediation and abiotic stress signalling. *Plant Biol* (Stuttg) **18**: 741–749.
- Plieth, C., Sattelmacher, B., and Hansen, U.-P.** (1997). Cytoplasmic Ca²⁺-H⁺-exchange buffers in green algae. *Protoplasma* **198**: 107–124.
- Poburko, D., Santo-Domingo, J., and Demarex, N.** (2011). Dynamic regulation of the mitochondrial proton gradient during cytosolic calcium elevations. *J. Biol. Chem.* **286**: 11672–11684.
- Rasi-Caldogno, F., Pugliarello, M.C., and De Michelis, M.I.** (1987). The Ca-transport ATPase of plant plasma membrane catalyzes a nH/Ca exchange. *Plant Physiol.* **83**: 994–1000.
- Sanders, D., and Slayman, C.L.** (1982). Control of intracellular pH. Predominant role of oxidative metabolism, not proton transport, in the eukaryotic microorganism *Neurospora*. *J. Gen. Physiol.* **80**: 377–402.
- Schönknecht, G., and Bethmann, B.** (1998). Cytosolic Ca²⁺ and H⁺ buffers in green algae: A comment. *Protoplasma* **203**: 206–209.
- Schwarzländer, M., Fricker, M.D., Müller, C., Marty, L., Brach, T., Novak, J., Sweetlove, L.J., Hell, R., and Meyer, A.J.** (2008). Confocal imaging of glutathione redox potential in living plant cells. *J. Microsc.* **231**: 299–316.
- Schwarzländer, M., Logan, D.C., Fricker, M.D., and Sweetlove, L.J.** (2011). The circularly permuted yellow fluorescent protein cpYFP that has been used as a superoxide probe is highly responsive to pH but not superoxide in mitochondria: Implications for the existence of superoxide “flashes.” *Biochem. J.* **437**: 381–387.
- Schwarzländer, M., Logan, D.C., Johnston, I.G., Jones, N.S., Meyer, A.J., Fricker, M.D., and Sweetlove, L.J.** (2012). Pulsing of membrane potential in individual mitochondria: A stress-induced mechanism to regulate respiratory bioenergetics in *Arabidopsis*. *Plant Cell* **24**: 1188–1201.
- Schwarzländer, M., Wagner, S., Ermakova, Y.G., Belousov, V.V., Radi, R., Beckman, J.S., Buettner, G.R., Demarex, N., Duchen, M.R., Forman, H.J., Fricker, M.D., and Gems, D., et al.** (2014). The “mitoflash” probe cpYFP does not respond to superoxide. *Nature* **514**: E12–E14.
- Serrano, R.** (1989). Structure and function of plasma membrane ATPase. *Annu. Rev. Plant Physiol. Plant Mol. Biol.* **40**: 61–94.
- Shih, H.W., Miller, N.D., Dai, C., Spalding, E.P., and Monshausen, G.B.** (2014). The receptor-like kinase FERONIA is required for mechanical signal transduction in *Arabidopsis* seedlings. *Curr. Biol.* **24**: 1887–1892.
- Shih, H.W., DePew, C.L., Miller, N.D., and Monshausen, G.B.** (2015). The cyclic nucleotide-gated channel CNGC14 regulates root gravitropism in *Arabidopsis thaliana*. *Curr. Biol.* **25**: 3119–3125.
- Stael, S., Wurzinger, B., Mair, A., Mehmer, N., Vothknecht, U.C., and Teige, M.** (2012). Plant organellar calcium signalling: An emerging field. *J. Exp. Bot.* **63**: 1525–1542.
- Swarbreck, S.M., Colaço, R., and Davies, J.M.** (2013). Plant calcium-permeable channels. *Plant Physiol.* **163**: 514–522.
- Sze, H., and Chanroj, S.** (2018). Plant endomembrane dynamics: Studies of K⁺/H⁺ antiporters provide insights on the effects of pH and ion homeostasis. *Plant Physiol.* **177**: 875–895.
- Sze, H., Liang, F., Hwang, I., Curran, A.C., and Harper, J.F.** (2000). Diversity and regulation of plant Ca²⁺ pumps: insights from expression in yeast. *Annu. Rev. Plant Physiol. Plant Mol. Biol.* **51**: 433–462.
- Tanaka, K., Swanson, S.J., Gilroy, S., and Stacey, G.** (2010). Extracellular nucleotides elicit cytosolic free calcium oscillations in *Arabidopsis*. *Plant Physiol.* **154**: 705–719.
- Tanaka, K., Choi, J., Cao, Y., and Stacey, G.** (2014). Extracellular ATP acts as a damage-associated molecular pattern (DAMP) signal in plants. *Front. Plant. Sci.* **3**: 446.
- Viotti, C., Luoni, L., Morandini, P., and De Michelis, M.I.** (2005). Characterization of the interaction between the plasma membrane H-ATPase of *Arabidopsis thaliana* and a novel interactor (PPI1). *FEBS J.* **272**: 5864–5871.
- Waadt, R., Krebs, M., Kudla, J., and Schumacher, K.** (2017). Multiparameter imaging of calcium and abscisic acid and high-resolution quantitative calcium measurements using R-GECO1-mTurquoise in *Arabidopsis*. *New Phytol.* **216**: 303–320.
- Wagner, S., Behera, S., De Bortoli, S., Logan, D.C., Fuchs, P., Carraretto, L., Teardo, E., Cendron, L., Nietzel, T., Füßl, M., Doccia, F.G., and Navazio, L., et al.** (2015a). The EF-hand Ca²⁺ binding protein MICU choreographs mitochondrial Ca²⁺ dynamics in *Arabidopsis*. *Plant Cell* **27**: 3190–3212.
- Wagner, S., Nietzel, T., Aller, I., Costa, A., Fricker, M.D., Meyer, A. J., and Schwarzländer, M.** (2015b). Analysis of plant mitochondrial function using fluorescent protein sensors. *Methods Mol. Biol.* **1305**: 241–252.
- Wagner, S., De Bortoli, S., Schwarzländer, M., and Szabò, I.** (2016). Regulation of mitochondrial calcium in plants versus animals. *J. Exp. Bot.* **67**: 3809–3829.
- Wang, W., Fang, H., Groom, L., Cheng, A., Zhang, W., Liu, J., Wang, X., Li, K., Han, P., Zheng, M., Yin, J., and Wang, W., et al.** (2008). Superoxide flashes in single mitochondria. *Cell* **134**: 279–290.
- Wirtz, M., and Hell, R.** (2003). Production of cysteine for bacterial and plant biotechnology: Application of cysteine feedback-insensitive isoforms of serine acetyltransferase. *Amino Acids* **24**: 195–203.
- Yang, D.L., Shi, Z., Bao, Y., Yan, J., Yang, Z., Yu, H., Li, Y., Gou, M., Wang, S., Zou, B., Xu, D., and Ma, Z., et al.** (2017). Calcium pumps and interacting BON1 protein modulate calcium signature, stomatal closure, and plant immunity. *Plant Physiol.* **175**: 424–437.
- Yang, Y., Hammes, U.Z., Taylor, C.G., Schachtman, D.P., and Nielsen, E.** (2006). High-affinity auxin transport by the AUX1 influx carrier protein. *Curr. Biol.* **16**: 1123–1127.
- Yu, H., Yan, J., Du, X., and Hua, J.** (2018). Overlapping and differential roles of plasma membrane calcium ATPases in *Arabidopsis* growth and environmental responses. *J. Exp. Bot.* **69**: 2693–2703.